Tunable non-equilibrium gating of flexible DNA nanochannels in response to transport flux

YOUDONG MAO[1,2], SONG CHANG[1], SHAOXUAN YANG[1], QI OUYANG[1]* AND LEI JIANG[3]*

[1]School of Physics and Center for Theoretical Biology, Peking University, Beijing 100871, China
[2]National Center for Nanoscience and Technology, Beijing 100080, China
[3]Institute of Chemistry, Chinese Academy of Sciences, Beijing 100080, China
*e-mail: qi@pku.edu.cn; jianglei@iccas.ac.cn

Published online: 27 May 2007; doi:10.1038/nnano.2007.148

Biological nanochannels made from proteins play a central role in cellular signalling[1–9]. The rapid emergence of DNA nanotechnology in recent years[10–13] has opened up the possibility of making similar nanochannels from DNA. Building on previous work on switchable DNA nanocompartment[14,15], we have constructed complex DNA nanosystems to investigate the gating behaviour of these nanochannels. Here we show that DNA nanochannels can be gated by stress exerted by permeating solute particles at non-equilibrium states due to the high flexibility of the nanochannels. This novel gating mechanism results in tunable ratchet-like transport of solute particles through the nanochannels. A simple model that couples non-equilibrium channel gating with transport flux can quantitatively explain a number of the phenomena we observe. With only one set of model parameters, we can reproduce diverse gating behaviours, modulated by an inherent gating threshold. This work could lead to the development of new devices based on DNA nanochannels.

The simple concept of active DNA nanocompartments (ADNCs)[14,15] is outlined in Fig. 1a. A compact array of short segments of double-stranded DNA (dsDNA) can form a switchable membrane, in which a nanocompartment is formed by means of a single-stranded DNA (ssDNA) spacer layer in the vicinity of the substrate surface. For clarity, the ensemble of densely packed dsDNA segments, (highlighted in green in the right of Fig. 1a), excluding the ssDNA spacers is referred to as the 'dsDNA membrane'. Previous studies have shown that the dsDNA membrane, at equilibrium states, is impermeable to solute particles $\sim$1 nm in size when the dsDNA has a fully complementary hybridization, whereas a single mutation in the fuel DNA means that a leakproof membrane cannot be formed[14,15]. In principle, the apertures lined by the juxtaposed nearest-neighbouring DNA duplexes in the dsDNA membrane may serve as single-file nanochannels for certain solute particles having sizes comparable to the channel diameters ($\sim$9–20 Å), as illustrated in Fig. 1b.

Our model nanosystem (Fig. 1a; see also Supplementary Information, Fig. S1) comprises two components: a DNA array possessing an ADNC nanostructure, and a 1,4-phenylenediisothiocyanate (PDC) self-assembled monolayer that can bind thionine molecules[16]. Because the reaction between PDC and thionine is reversible and exothermic (Fig. 1c; see also Supplementary Information, Fig. S2), the PDC monolayer can be used to store and release thionine, controlled by changes in temperature (Fig. 1d, solid black line). This feature enables us to regulate thionine concentrations inside the ADNCs using the PDC monolayer, providing a means of triggering thionine permeation across the dsDNA channels.

To drive the thionine molecules to move across the dsDNA channels, we first let the PDC monolayer store thionine to saturation, with the ADNC in the open state, and then close the ADNC at T_c in the presence of thionine, where T_c is defined as the switching temperature at which the ADNC is closed fully by hybridization. Under this condition, we profile the surface concentration (Γ) of thionine confined inside the ADNC by electrochemical methods[14–16], while increasing the system temperature at a rate of $\sim$2–5 °C per 30 min starting from 0 °C (see Methods). During the course of Γ–T profiling, the thionine concentration in the external solution is maintained at a constant value ($C_2 = 10\ \mu$M). Meanwhile, the thionine concentration inside the ADNC (denoted as $C(t)$) is controlled by both the PDC monolayer and the gating of DNA channels. Typical Γ–T profiles (Fig. 1d) exhibit a stepwise decrease with increasing temperature. The sustained concentration in a plateau indicates that the DNA channels of the closed state prevent thionine from diffusing out of the ADNC, whereas the sudden drop between contiguous plateaux indicates that the DNA channels are opened during the measurement step, allowing the thionine to permeate into the external solution. The alternating transition between plateaux and sudden drops in the same Γ–T profiles implies ratchet-like, intermittent, controlled release of thionine through the DNA channels. Figure 1d also clearly shows that increasing T_c results in the decrease of both the maximum and the step number of the Γ–T profiles, suggesting that T_c can be used to modulate the behaviour of the profiles. Four control experiments (see Methods), which all show nonlinear decay (typically shown as the solid black line of Fig. 1d) and correspond to the situation in which neither the closed-state ADNC nanostructure nor the DNA channel is well formed, confirm that the stepwise effect can only arise from the gating of DNA channels.

To quantitatively explain our experimental observations, we established a simple theoretical model based on stochastic

©2007 Nature Publishing Group

dynamics. The gating of DNA channels is described as a diffusion-limited process[6–8]. Two major factors are considered in the model: a stress $F(t)$ arising from permeating thionine molecules acting on the inner surface of a channel, and an energy landscape describing nanomechanical deformation potential during the channel gating. According to our estimation, the timescale of channel gating is much larger than that of the transport of thionine (see Supplementary Information, Note S1). The screened long-range electrostatic interaction between dsDNA molecules[17,18] entails high flexibility[19] of the DNA channels, so the energy landscape of the DNA channels can be described in terms of the channel's radius (R) as an upward parabola, as shown in Fig. 2a (see Methods and Supplementary Information, Note S2). Using this knowledge, we find the equation governing the channel's motion (see Supplementary Information, Note S3) to be

$$\frac{\partial\langle x(t)\rangle}{\partial t} = -\beta D(2\pi\alpha\langle x(t)\rangle - F(t)) \qquad (1)$$

where $\langle x(t)\rangle$ is the mean of $x(t) = R(t) - R_0$ over thousands of individual motion trajectories, R_0 is the radius of a free channel of ground energy in equilibrium, D is the conformational diffusion coefficient, α is the area tension on the circumference of the channel, and $\beta = 1/(k_B T)$. Taking into account the single-file nature of thionine permeation through the DNA channels (see Supplementary Information, Note S4), our simulation with a one-dimensional lattice model[20] establishes a relationship between $F(t)$ and $C(t)$ (see Fig. 2b; see also Supplementary Information, Note S5)

$$F(t) \approx \frac{pn_m C(t)}{C(t) + \kappa^{-1}} \qquad (2)$$

where p is the mean stress of single thionine acting on the inner surface of the channel, n_m is the maximum of the mean residence number of permeating thionine inside the channel, and κ is the association constant. This equation reflects the spontaneous change of channel–particle interactions in response to transport flux.

Because the static channel–particle interactions can be simulated by a steep-wall potential[21] (see Supplementary Information, Note S6), there exists a critical radius R^* such that, if $R(t) < R^*$, the channel–particle interactions provide sufficiently large frictions to inhibit the thionine in moving along the channel, resulting in single-channel transport flux $j(t) = 0$. If $R(t) > R^*$, the channel–particle interactions only generate a small viscous friction, γ, allowing the thionine to permeate with $j(t) > 0$. Given that the average spacing between opened channels in the dsDNA membrane is relatively large (estimated to be ~69 μm, using data shown in Table 1), the interaction between the opened channels can be neglected. Assuming that the dsDNA membrane and the PDC monolayer are homogeneous with respect to their densities[14,15], all DNA channels in the same dsDNA membrane statistically face the same conditions, meaning that the gatings of the DNA channels behave in concert. Based on this scenario, because $j(t)$ is approximately a linear function of $C(t)$ at steady states[22–24], $C(t)$ can be analytically solved. With this information it is possible to resolve numerically the motion trajectories of the DNA channels corresponding to our real experiments (see Methods and Supplementary Information, Note S7).

Figure 2c depicts numerically one complete cycle of thionine pumping through a single DNA channel against the nanomechanical deformation potential of the channel. The simultaneous motion trajectories of $\langle x(t)\rangle$ coupled to $F(t)$ and $C(t)$ are depicted in Fig. 2d and e, respectively. The hysteretic trajectory maps the critical radius at $\langle x(t)\rangle = R^* - R_0$ to dual criticality of concentrations (Fig. 2e). In other words, C_o corresponds to the opening criticality of the channel during the increase of $C(t)$, and C_c corresponds to the closing criticality

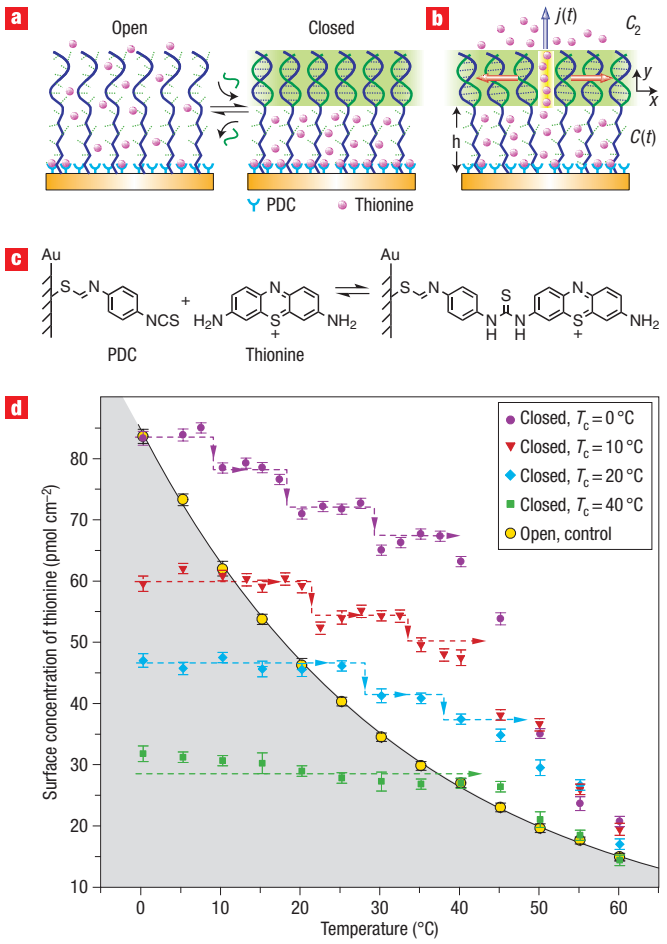

Figure 1 Experimental observations of ratchet-like thionine transport through DNA nanochannels. a, Schematic of the DNA nanosystem incorporating ADNCs. Switching of an ADNC between open (left) and closed (right) states can be carried out by hybridization and denaturation processes[14]. At the bottom of the ADNC is a PDC self-assembly monolayer. The key shows the graphic representations of PDC and thionine. **b**, Schematic of single-file transport of thionine molecules through a transiently opened DNA channel. **c**, Chemical reaction of surface-bound PDC with thionine. **d**, Surface concentration of thionine molecules plotted as a function of temperature ($\Gamma - T$ profiles). The profile of the open state (as control) is fitted with simple exponential decay (solid line). The dashed lines for the closed state are calculated according to our model. Arrows show the direction of time evolution of measurements. Because the PDC monolayer cannot store more thionine after the ADNC is closed at T_c, the maximum value of each $\Gamma - T$ profile of the closed state approximates the Γ value at T_c in the open-state curve and decreases with increasing T_c. Thus, the $\Gamma - T$ profiles of the closed state all show sustained level in the grey area, and the stepwise effect can only happen in the white area. Above the melting temperature (~48 °C) of the dsDNA segment, all profiles of the closed-state ADNC converge to the same level as a result of dsDNA denaturation, which may open the ADNC and deform the DNA channels.

©2007 Nature Publishing Group

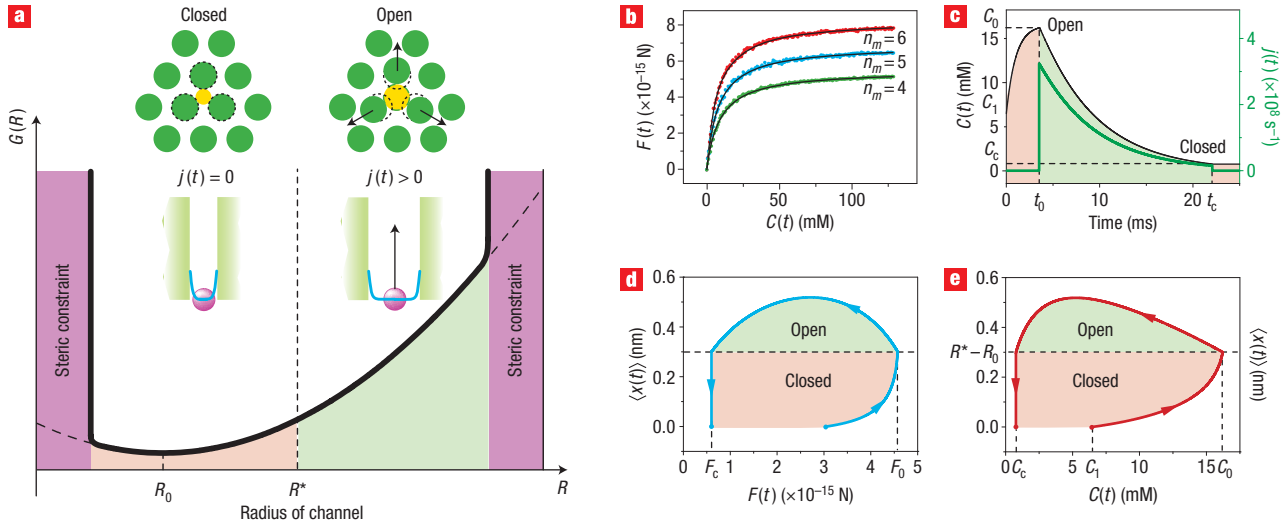

Figure 2 Theoretical modelling of the gating dynamics of DNA channels. a, The energy landscape of a DNA channel is represented by a thick solid line, with the minimum located at the abscissa of R_0. The two regions corresponding to the closed and open states of the channel respectively are separated by the dashed line at the abscissa of R^*. Upper inset: Top view of the closed (left) and open (right) DNA channel marked by yellow. For illustration, it is assumed that the dsDNAs are packed in a hexagonal lattice. Lower inset: Lateral view of closed (left) and open (right) DNA channels. The purple spheres represent thionine, blue lines represent the steep-wall potential between thionine and the DNA channel, and the arrow shows the direction of thionine transport flux. **b**, Simulated mean stress of thionine molecules exerted on the inner surface of the DNA channels as a function of thionine concentration inside the ADNCs. The black lines fit equation (2). Results for three different lengths of DNA channels are shown, corresponding to 8*r*, 10*r* and 12*r* from bottom to top, respectively, where *r* is the radius of thionine. **c**, A complete cycle of thionine pumping coupled with single channel gating. Black and green lines show respectively the time evolution of $C(t)$ and that of $j(t)$. **d**, The mean trajectory of $\langle x(t)\rangle$ as a function of $F(t)$. **e**, The mean trajectory of $\langle x(t)\rangle$ as a function of $C(t)$. Data shown in **c**–**e** were simultaneously obtained from the same run of numerical computation from our model, using the parameters shown in Table 1. Through hysteresis, the critical radius determines two critical forces (F_o, F_c) in **d** and two critical concentrations (C_o, C_c) in **e**. In all panels **c**–**e**, light red and light green mark the closed and open states of the channels respectively. At the beginning of the cycle, because $C(0) = C_1 < C_o$, the channels are closed during the time $t < t_o$. The increase of $C(t)$ elevates the stress of the solute particles acting on the channel's surface. When $C(t)$ reaches $C(t_o) = C_o = 16.22$ mM at $t = t_o$, the channel radius reached the critical radius of $R^* = R_0 + 0.3$ nm, thus opening the channels and enabling transport flux $j(t)$. As a result, $C(t)$ tends to decease until $t = t_c$, where $C(t_c) = C_c = 0.77$ mM.

Table 1 Parameter values used in calculations.

Parameter	Value
Conformational diffusion coefficient of the channels (D)	10^{-13} m^2 s^{-1}
Critical radius of channel gating (R^*)	1 nm
Area tension of single channel at 0 °C (α)	($\sim$0.89–1.19) $\times$ 10^{-6} J m^{-2}
Length of the channels (L)	$\sim$5.5 nm
Effective height of ADNCs (h)	$\sim$5 nm
Density of simultaneously opened DNA channels (N_0)	$\sim$2.1 $\times$ 10^4 cm^{-2}
Density of free DNA channels in equilibrium (ρ_0)	($\sim$0.6–1.0) $\times$ 10^{13} cm^{-2}
Radius of thionine molecule (r)	0.55 nm
Thionine concentration when the ADNC is just closed (C_1)	6.5 mM
Thionine concentration in the external solution (C_2)	10 μM
Stress of single thionine exerting on channel surface (p)	$\sim$1.37 $\times$ 10^{-15} N
Maximum number of thionine inside the channel (n_m)	5
Associate constant of thionine inside a channel (κ)	125 M^{-1}
Relaxation time of thionine release from PDC monolayer (τ)	2 ms
$j(t)$ parameters in equation (5) (A_1, A_2)	$A_1 = 2 \times 10^{10}$ (M s)$^{-1}$; $A_2 = 2A_1$

All simulations shown in Fig. 4 share the same parameter set listed herein. The parameters, based on available physical or chemical information, are fixed in all simulations, except the C^* function. The changes of C^* behaviour (Fig. 3) modulate the diverse gating behaviours (Fig. 4). However, the first-type simulations of different T_c, shown in Fig. 4a, Fig. S3 and Fig. S4, use the same C^* function. Note that the C^* function is changed using α and R_0 according to equation (3), whereas α and R_0 are both the functions of dsDNA surface density (ρ), and are used according to experimental setup. No free parameter appears in our modelling. For more details, see Supplementary Information, Notes S8 and S9.

of the channel during the decrease of $C(t)$. Most importantly, $h(C_o - C_c)$ measures the net quantity of thionine permeating through the channel during such a pumping cycle, where h is the effective height of the ADNC. To directly simulate the Γ–T profiles, we notice that equations (1) and (2) give a threshold concentration

$$C^* = \kappa^{-1}\{pn_m/[2\pi\alpha(R^* - R_0)] - 1\}^{-1} \qquad (3)$$

which provides a general criterion for channel gating: the channels can be opened only if C_{max} is larger than C^*, where C_{max} is the maximum value of $C(t)$ after the increase in temperature triggers the release of thionine from the PDC monolayer. The criterion is well verified by our numerical simulations (data not shown). Figure 3 summarizes the relationships between C^* and C_{max} during the Γ–T profiling, suggesting five possible cases, as discussed in the following and in the legend of Fig. 3.

Figure 4 shows quantitative comparisons of simulations and experiments on a variety of typical Γ–T profiles using the same parameter set shown in Table 1. It suggests that the behaviour of Γ–T profiles may be classified into two major types. The first type corresponds to $C^* > C_{max}$ in the temperature range of interest (blue line of Fig. 3). As the release of thionine from the PDC monolayer in a temperature change of 5 °C is not always enough to increase $C(t)$ to overwhelm C^*, the channels cannot be opened in every measurement step of the Γ–T profiles, resulting in the stepwise effect (Fig. 4a; see also Supplementary

©2007 Nature Publishing Group

Information, Figs S3 and S4). The second type corresponds to $C^* < C_{max}$ in the temperature range of interest (green line of Fig. 3). In this case, the DNA channels can be opened in every measurement step, leading to a linear decrease in the $\Gamma-T$ profiles (Fig. 4b). In addition to these two discrete types, it is possible to observe both stepwise and linear-decrease effects in the same $\Gamma-T$ profiles, as they arise from the crossovers of C^* and C_{max} in the temperature range of interest. Figure 4c demonstrates that a crossover of $C^* = C_{max}$ taking place at $T = T^*$ (red line of Fig. 3) results in the first type of behaviour at $T < T^*$ and the second type of behaviour at $T > T^*$. Similar results with the reverse sequence of behaviours are also observed (see Supplementary Information, Fig. S5), corresponding to the case of $C^* < C_{max}$ at $T < T^*$ (dashed red line in Fig. 3). Furthermore, two crossovers of C^* and C_{max} (orange line in Fig. 3) give rise to a stepwise behaviour sandwiched within the linear-decrease behaviour in the $\Gamma-T$ profile (Fig. 4d). All possible kinds of $\Gamma-T$ profiles predicted by our model quantitatively agree with experimental observations. This strongly validates our analyses of DNA channel gating.

The mechanism of DNA channel gating is remarkably distinct from the gating mechanisms of protein channels. First, unlike the bistable nature of protein channel gating, in which both the open and closed conformations have different local stable states[3–8], the DNA channels show no bistability. A free DNA channel in equilibrium corresponds to the ground energy, which represents a stable closed state (Fig. 2a). Only when the DNA channel dilates under the stress from permeating solute molecules to reach a critical radius is the channel permeable to the solute. The open state of the DNA channels is far away from equilibrium, showing a highly active trend towards closing. Second, protein channels are formed by rigid binding (short-range interaction) between subunits, so they are usually gated by means of membrane voltage or membrane tension rather than transport flux[1–9]. Our findings suggest that the DNA channels are gated by the channel–particle interactions owing to their high flexibility. The calculations presented in Figs 2 and 4 demonstrate that spatiotemporal coupling of DNA channel gating with transport flux involves spontaneous periodic changes of the channel–particle interaction force $F(t)$ at non-equilibrium states, which gives rise to asymmetric periodic oscillation of $C(t)$, $j(t)$ and $R(t)$, indicating a ratchet-like mechanism[25,26] for both channel gating and solute permeation (see Supplementary Information, Discussion, for details).

The unique flexibility of DNA channels discovered here has not ever been seen in known nanochannels[27] formed by molecular sieves[28], synthetic nanopores[26] and carbon nanotubes[29]. Our recent work has demonstrated that the ADNCs can be largely improved using four-stranded non-Watson–Crick DNA structures[15]. This means that flexible DNA channels may also be formed by reconstruction of other DNA nanoarchitectures[13], but not restricted to the Watson–Crick duplex used in this work. Our modelling provides a general framework for the *in silico* rational design of such DNA channel systems, where the physical properties of DNA channels may be programmed by means of DNA sequences and nanostructures. The novel gating mechanism of DNA channels also suggests unique potential applications. For instance, the DNA channels may be constructed on the surfaces of micro- or nanocrystal antennas, where the local temperature can be controlled remotely by inductive coupling of a radio-frequency magnetic field to the antenna[30]. This may be used to develop remotely tunable controlled release of small molecules through DNA channels, which has great potential in drug delivery and nanomedicine. Furthermore, the DNA channels may be readily integrated into micro- and nanofluidics systems, serving as nanoscale, controlled-release subunits for enabling novel applications.

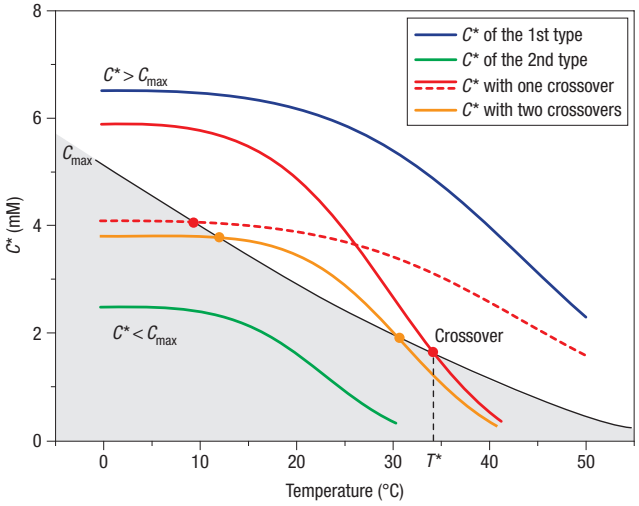

Figure 3 Behaviour of the gating threshold C^* in relation to C_{max}. The solid black line sketches the maximum concentration (C_{max}) of thionine in a closed ADNC with all DNA channels closed. (See Supplementary Information, Note S8 for the detailed methods used to determine C^* and C_{max} as functions of temperature.) The grey area marks the regime where $C^* < C_{max}$. The blue line demonstrates the case of $C^* > C_{max}$ within the temperature range of interest, which gives rise to the first type of behaviour of the $\Gamma-T$ profiles. The green line demonstrates the case of $C^* < C_{max}$ within the temperature range of interest, which gives rise to the second type of behaviour of the $\Gamma-T$ profiles. The solid red line demonstrates the case of the mixed type, which shows one crossover at T^* between C^* and C_{max}, with $C^* > C_{max}$ at $T < T^*$, so that the corresponding $\Gamma-T$ profiles show the first type of behaviour at $T < T^*$, but the second type of behaviour at $T > T^*$. The dashed red line demonstrates another case of one crossover between C^* and C_{max}, with $C^* < C_{max}$ at $T < T^*$, which gives the reverse sequence of first and second types of behaviour in the corresponding $\Gamma-T$ profiles. The orange line demonstrates the case of the mixed type with two crossovers, at T_1^* and T_2^* ($T_1^* < T_2^*$), so that the corresponding $\Gamma-T$ profiles show the first type of behaviour in the range $T_1^* < T < T_2^*$ and the second type in the range $T < T_1^*$ and $T > T_2^*$.

METHODS

SYSTEM PREPARATION

Preparation of the experimental setup involved two steps. First, we prepared ADNCs on gold substrates as described elsewhere[14]. The ADNCs were then further assembled with PDC by washing with 30% urea to denature the dsDNA and rinsing with double distilled water and *N*,*N*-dimethylformamide (DMF) several times, and then exposure to 0.2% PDC solution (10% pyridine/DMF) for 24 h at room temperature. The typical DNA sequences used were (1) 5′-$(A)_{10}$-CTGAGGAGGGGCCAGA-3′ and (2) 5′-$(A)_{10}$-GGAGGTGAGTCGCTAGC-3′. The complementary strands containing a wobble base were 5′-TCTGGCCXCTCCTCAG-3′, where X = C for the perfectly complementary strands, and X = A, G or T for the single-base mismatched strands.

$\Gamma-T$ PROFILES

To allow the PDC monolayer to bind with thionine to saturation, the device at the open state was exposed to 20 μM thionine in Tris–HCl buffer (pH 8) for 1 h in order to accumulate thionine at room temperature. To turn on the ADNC, the

©2007 Nature Publishing Group

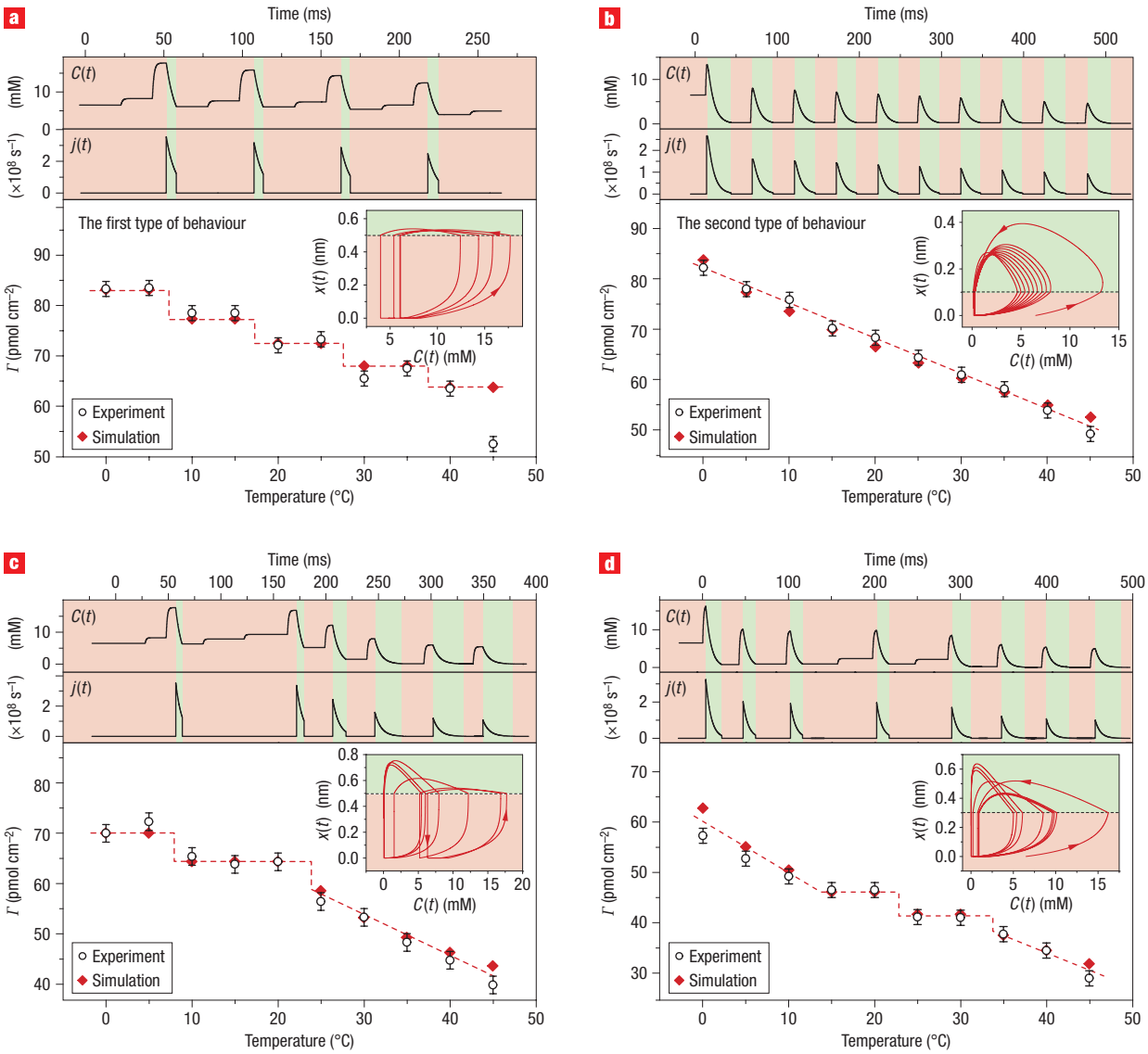

Figure 4 Modulation of gating behaviours of DNA channels. a, The first type of behaviour of the $\Gamma-T$ profile is reproduced from simulation to show a stepwise decrease for $C^* > C_{max}$. **b**, The second type of behaviour of the $\Gamma-T$ profile is reproduced from simulation to show a linear decrease for $C^* < C_{max}$. **c**, The mixed behaviour in the case of one crossover between the curves of C^* and C_{max} at $T = T^*$ (~25 °C) is reproduced from simulation to be a stepwise decrease in the range $T < T^*$ and a linear decrease in the range $T > T^*$. **d**, The mixed behaviour in the case of two crossovers between the curves of C^* and C_m at $T = T_1^*$ (~13 °C) and $T = T_2^*$ (~33 °C) is reproduced from simulation to show a stepwise decrease in the range $T_1^* < T < T_2^*$ and a linear decrease in the ranges $T < T_1^*$ and $T > T_2^*$. All experiments shown here are obtained with $T_c = 0$ °C (results for other values of T_c are shown in the Supplementary Information, Figs S3 and S4). In each figure, the upper and middle, and bottom panels show, respectively, the computed temporal evolutions of $C(t)$ and $j(t)$, and the comparison between the simulated $\Gamma-T$ profile (filled diamonds) and the experimentally measured $\Gamma-T$ profile (open circles). The insets show the mean trajectory of the channel's reaction coordinate, with the first cycle marked by arrows; light red and light green mark the closed and open states of the channels, respectively. Data shown in the same figure are all obtained simultaneously from the same run of the simulations. The parameters used are shown in Table 1. Note that the experimental observations in **b**–**d** were achieved by slightly decreasing dsDNA density or ionic strength relative to the experimental setup of **a**, which presents smaller C^* according to equation (3) (see Supplementary Information, Note S9).

device in the open state was incubated in a hybridization buffer containing 5 μM complementary DNA strands (Tris–HCl buffer, pH 7.8, 100 mM NaCl, 1 mM $MgCl_2$ and 10 μM thionine), with the ambient temperature annealed from 60 °C to T_c within 10 min, and then sustained at T_c for ~12 h. The ambient temperature was controlled by a thermostat.

After the device switched on at T_c, the Γ values were repeatedly measured by cyclic voltammetry (CV) as the temperature increased from 0 to 60 °C at a rate of ~2–5 °C every 30 min. Specifically, after each measurement the temperature was increased ~2–5 °C within 1 min, and maintained at the same temperature for 30 min to facilitate a sufficient system equilibration before the next measurement. The thionine outside the ADNCs was washed away before each CV measurement. The electrochemical analysis was conducted in a three-electrode system using a model 660 A electrochemical workstation (CH Instruments), with an Ag/AgCl reference electrode, a platinum counter electrode and an ADNC-modified gold surface as the working electrode. The surface area of the ADNC-modified working electrode examined was 0.03 cm^2. The

©2007 Nature Publishing Group

electrolyte used in the three-electrode system was 20 mM Tris–HCl (pH 8) containing 1 mM $MgCl_2$. In the CV, the potential versus Ag/AgCl was swept from −0.4–0 V with a scan rate 0.1 V s^{-1}. The surface concentrations of thionine on the electrode surface were calculated as described elsewhere[14]. The system was immediately returned to the operation solution (Tris–HCl buffer, pH 7.8, 100 mM NaCl, 1 mM $MgCl_2$ and 10 μM thionine) to recover its equilibrium after each measurement.

Control experiments were carried out (1) using single mismatched strands, instead of perfect complements, to switch on the ADNC, (2) with the open-state ADNCs in which all DNA were single strands, (3) on a device with very low density ($<10^{11}$ molecules per cm^2) DNA array, and (4) on a pure PDC monolayer in the absence of ADNC. The first case yielded a low hybridization efficiency of less than 50%, leading to a substantially incomplete dsDNA membrane. The other three cases correspond to the situation where no DNA channel is formed because of the absence of the dsDNA membrane.

ENERGY LANDSCAPE OF DNA CHANNELS

The deformation potential of a single DNA channel can be written explicitly in terms of the channel's radius (R) as

$$G(R) = \alpha\pi R^2 - f2\pi R + G_0 \tag{4}$$

where α and f represent, respectively, the area tension and the line tension on the circumference of the channel that do not explicitly depend on R, and G_0 is a radial-independent contribution to the deformation energy. A free channel at the equilibrium state corresponds to the ground energy of $G_0 - \pi f^2/\alpha$ with $R_0 = f/\alpha$. (For more details, see Supplementary Information, Note S2.)

THEORETICAL MODELLING

The brownian motion of a thionine molecule along the channel is described by Langevin dynamics under a potential $U(y)$ in the overdamped limit[22–24]. Solving the corresponding Fokker–Plank equation, the resulting local instantaneous flux of thionine molecules through a single channel is

$$j(t) = A_1 C(t) - A_2 C_2 \tag{5}$$

where $A_i = \frac{\varepsilon}{\gamma} e^{U(y_i)/\varepsilon}\left[\int_{y_1}^{y_2} e^{U(y)/\varepsilon} dy\right]^{-1}, i = 1, 2, C_2$ is the thionine concentration in external solution and $\varepsilon = k_B T/m$. The detailed calculation of equation (5) is extensively given in ref. 22. As shown in Fig. 2c, at $t = t_o$, the channels are opened with thionine transport flux established. In the interval $t_o < t < t_c$, the change of $C(t)$ due to the steady-state flux is $dC(t) = -j(t)N(t)V^{-1}\,dt$, where $N(t)$ is the total number of the open channels that do not explicitly depend on $C(t)$, and V is the effective volume of the reservoir in the ADNCs. However, the PDC monolayer releases thionine with increasing temperature, thus affecting $C(t)$ by $dC(t) = C_m \tau^{-1} e^{-t/\tau} dt$, as observed experimentally (see Supplementary Information, Fig. S2), where C_m and τ are parameters of the amplitude and the relaxation time, respectively. One obtains the differential equation describing $C(t)$ by the addition of the contribution of the steady-state flux and that of the thionine source

$$\frac{d}{dt}C(t) = C_m \tau^{-1} e^{-t/\tau} - j(t)N(t)V^{-1}. \tag{6}$$

Inserting equation (5) into equation (6), and considering the initial condition $C(t) = C_o$, one may find the exact solution of $C(t)$ in the interval $t_o < t < t_c$

$$C(t) = e^{-T(t)}\left\{\int_{t_o}^{t}\left[\frac{C_m}{\tau}e^{-t'/\tau} + \frac{A_2 C_2}{V}N(t')\right]e^{T(t')}\,dt' + C_o\right\} \tag{7}$$

where $T(t) = (A_1/V)\int_{t_o}^{t} N(t')\,dt'$. The flux $j(t)$ can be immediately obtained by inserting equation (7) into (5). (For more details and simulation methods for Γ–T profiles, please see Supplementary Information, Notes S7–S9.)

Received 17 February 2007; accepted 27 April 2007; published 27 May 2007.

References

1. Hille, B. *Ion Channels of Excitable Membranes* (Sinauer Associates, Sunderland, 2001).
2. Gillespie, P. G. & Walker, R. G. Molecular basis of mechanosensory transduction. *Nature* **413,** 194–202 (2001).
3. Yellen, G. The voltage-gated potassium channels and their relatives. *Nature* **419,** 35–42 (2002).
4. MacKinnon, R. Potassium channels and the atomic basis of selective ion conduction (Nobel lecture). *Angew. Chem. Int. Edn* **43,** 4265–4277 (2004).
5. Perozo, E., Cortes, D. M., Sompornpisut, P., Kloda, A. & Martinac, B. Open channel structure of MscL and the gating mechanism of mechanosensitive channels. *Nature* **418,** 942–948 (2002).
6. Goychuk, I. & Hänggi, P. Ion channel gating: a first-passage time analysis of the Kramers type. *Proc. Natl Acad. Sci. USA* **99,** 3552–3556 (2002).
7. Wiggins, P. & Phillips, R. Analytic models for mechanotransduction: Gating a mechanosensitive channel. *Proc. Natl Acad. Sci. USA* **101,** 4071–4076 (2004).
8. Markin, S. & Sachs, F. Thermodynamics of mechanosensitivity. *Phys. Biol.* **1,** 110–124 (2004).
9. VanDongen, A. M. J. K channel gating by an affinity-switching selectivity filter. *Proc. Natl Acad. Sci. USA* **101,** 3248–3252 (2004).
10. Seeman, N. C. DNA nanotechnology: Novel DNA constructions. *Annu. Rev. Biophys. Biomol. Struct.* **27,** 225–248 (1998).
11. Seeman, N. C. DNA in a material world. *Nature* **421,** 427–431 (2003).
12. Yan, H. Nucleic acid nanotechnology. *Science* **306,** 2048–2049 (2004).
13. Feldkamp, U. & Niemeyer, C. M. Rational design of DNA nanoarchitectures. *Angew. Chem. Int. Edn* **45,** 1856–1876 (2006).
14. Mao, Y. *et al.* Reversibly switchable DNA nanocompartment on surfaces. *Nucleic Acids Res.* **32,** e144 (2004).
15. Mao, Y. *et al.* Alternating-electric-field-enhanced reversible switching of DNA nanocontainers with pH. *Nucleic Acids Res.* **35,** e33 (2007).
16. Mao, Y., Luo, C. & Ouyang, Q. Studies of temperature-dependent electronic transduction on DNA hairpin loop sensor. *Nucleic Acids Res.* **31,** e108 (2003).
17. Cherstvy, A. G., Kornyshev, A. A. & Leikin, S. Torsional deformation of double helix in interaction and aggregation of DNA. *J. Phys. Chem. B* **108,** 6508–6518 (2004).
18. Kornyshev, A. A. & Leikin, S. Sequence recognition in the paring of DNA duplexes. *Phys. Rev. Lett.* **86,** 3666–3669 (2001).
19. Wiggins, P. A. *et al.* High flexibility of DNA on short length scales probed by atomic force microscopy. *Nature Nanotech.* **1,** 137–141 (2006).
20. Chou, T. How fast do fluids squeeze through microscopic single-file pores? *Phys. Rev. Lett.* **80,** 85–88 (1998).
21. Hahn, K., Kärger, J. & Kukla, V. Single-file diffusion observation. *Phys. Rev. Lett.* **76,** 2762–2765 (1996).
22. Eisenberg, R. S., Klosek, M. M. & Schuss, Z. Diffusion as a chemical reaction: Stochastic trajectories between fixed concentrations. *J. Chem. Phys.* **102,** 1767–1780 (1995).
23. Nadler, B., Schuss, Z. & Singer, A. Langevin trajectories between fixed concentrations. *Phys. Rev. Lett.* **94,** 218101 (2005).
24. Kosztin, I. & Schulten, K. Fluctuation-driven molecular transport through an asymmetric membrane channel. *Phys. Rev. Lett.* **93,** 238102 (2004).
25. Chinappi, M. *et al.* Molecular dynamics simulation of ratchet motion in an asymmetric nanochannel. *Phys. Rev. Lett.* **97,** 144509 (2006).
26. Siwy, Z., Fuliński, A. & Martin, C. R. Fabrication of a synthetic nanopore ion pump. *Phys. Rev. Lett.* **89,** 198103 (2002).
27. Dekker, C. Solid-state nanopores. *Nature Nanotech.* **2,** 209–215 (2007).
28. Chou, T. & Lohse, D. Entropy-driven pumping in zeolites and biological channels. *Phys. Rev. Lett.* **82,** 3552–3555 (1999).
29. Hummer, G., Rasaiah, J. C. & Noworyta, J. P. Water conduction through the hydrophobic channel of a carbon nanotube. *Nature* **414,** 188–190 (2001).
30. Hamad-Schifferli, K., Schwartz, J. J., Santos, A. T., Zhang, S. & Jacobson, J. M. Remote electronic control of DNA hybridization through inductive coupling to an attached metal nanocrystal antenna. *Nature* **415,** 152–155 (2002).

Acknowledgements

We thank A. G. Cherstvy for a critical review and helpful comments on the manuscript. This work is partly supported by the Ministry of Science and Technology of China, and the Chinese Natural Science Foundation.
Correspondence and requests for materials should be addressed to Q.O. and L.J.
Supplementary information accompanies this paper on www.nature.com/naturenanotechnology.

Author contributions

Y.M. designed the experiments, established the theoretical model and performed the numerical calculations. Y.M. and S.Y. carried out the experiments. Y.M. and Q.O. analysed the data. S.C. and Y.M. performed the simulation on the mean residence number of solute particle inside channels. Y.M. wrote the manuscript, and Q.O. and L.J. proofread it. Q.O. and L.J. supervised the research project.

Competing financial interests

The authors declare no competing financial interests.

Reprints and permission information is available online at http://npg.nature.com/reprintsandpermissions/

©2007 Nature Publishing Group

Supplementary Information

For

Tunable nonequilibrium gating of flexible DNA nanochannels in response to transport flux

Youdong Mao[1,2], Song Chang[1], Shaoxuan Yang[1], Qi Ouyang[1], Lei Jiang[3]

[1]School of Physics and Center for Theoretical Biology, Peking University, Beijing 100871, China

[2]National Center for Nanoscience and Technology, Beijing 100080, China

[3]Institute of Chemistry, Chinese Academy of Sciences, Beijing 100080, China

© 2007 **Nature Publishing Group**

Table of Contents

© 2007 Nature Publishing Group

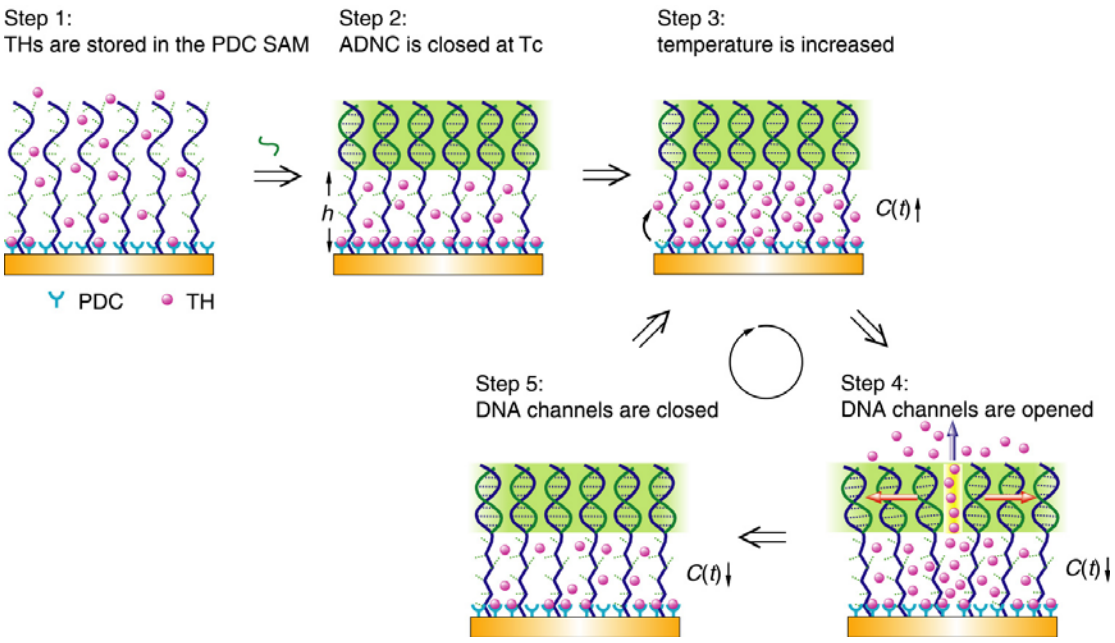

Supplementary Figure S1. Schematic drawing of experimental assay to drive the transient opening of DNA channels. In the 1st step, the thionine molecules are stored in the PDC monolayer with ADNC opened. In the 2nd step, the ADNC is closed at T_c, which gives rise to the maximum number of thionine confined inside the ADNC. In the 3rd step, the temperature is increased, which results in the thionine release from PDC monolayer. In the 4th step, the DNA channels are opened if elevated $C(t)$ could overwhelm C^*, resulting in the thionine loss of $h(C_o - C_c)$ from the ADNC. In the 5th step, the DNA channels are closed when $C(t)$ decreased to C_c. The 3rd, 4th, and 5th steps are cycled by further increasing temperature. One complete cycle formed by the contiguous 3rd, 4th, and 5th steps corresponds to a measurement of Γ data of a temperature during the Γ-T profiling. Therefore, the Γ-T profiles do not trace the detailed trajectories of $j(t)$ or $C(t)$, but instead, measure the resulting $h(C_o - C_c)$. Whereas direct measurement of single-channel flux on dsDNA membrane seems impossible by patch-clamping technique used in single-channel recording of protein channels in lipid-bilayer membrane, our assay avoids the technical difficulties of single-channel tracking but can still capture the unique gating behaviors of DNA channels.

© 2007 Nature Publishing Group

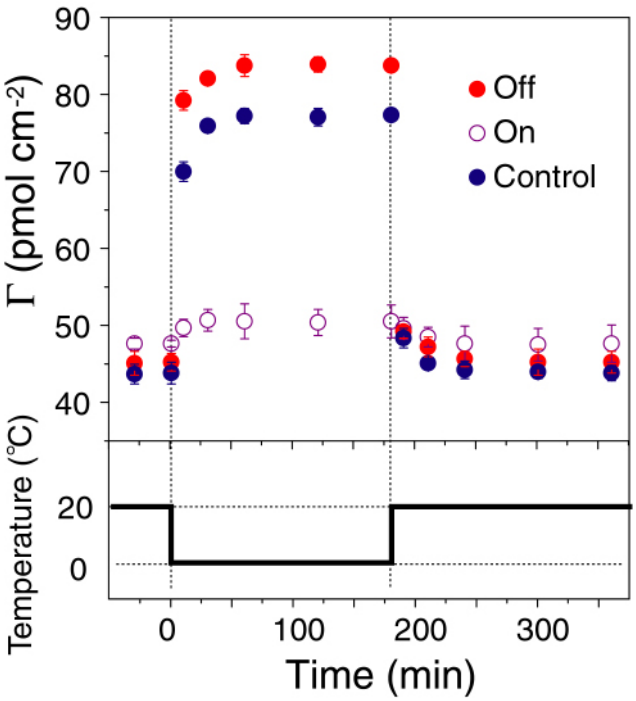

Supplementary Figure S2. Kinetics of thionine release from PDC monolayer. The jump of temperature can trigger the PDC monolayer to release (or absorb) the thionine to (from) the nearby solution. Its behaviors can be simply described as $C(t) = C_m(1 - \exp(-t/\tau)) + C_1$ in our modeling, which may provide a good approximation to the real experiments. The corresponding differential form is $dC(t) = C_m\tau^{-1}\exp(-t/\tau)dt$, which is also used in the theoretical analysis of this work.

© 2007 **Nature Publishing Group**

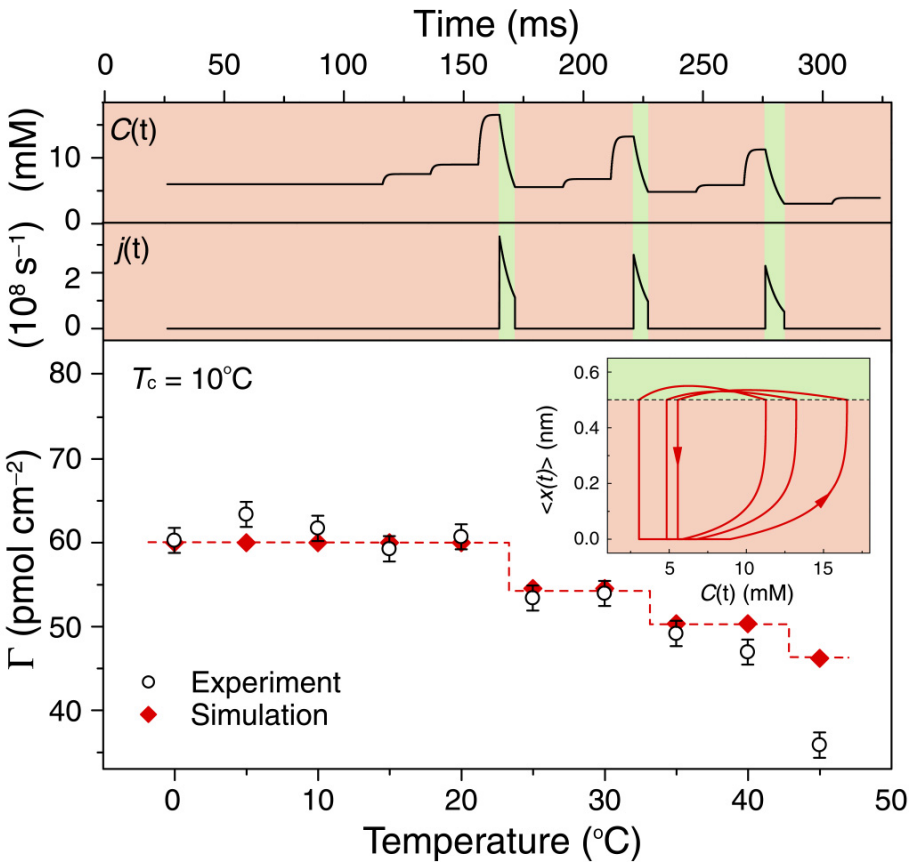

Supplementary Figure S3. Simulation of *Γ*-*T* profile of T_c = 10 ˚C, with compared to experiment. Below T_c = 10˚C the *Γ*-*T* profile should be sustained at a constant level, as observed experimentally, because after the ADNC is closed at T_c = 10˚C the PDC monolayer cannot store more thionine molecules and the maximum thionine quantity stored in the PDC monolayer is controlled by the *Γ*-*T* profile of the open state ADNC (Fig. 1d in the main paper, control, black line). The upper panel shows the calculated time evolution of *C*(t) corresponding to the simulation of *Γ*-*T* profile; the middle panel shows the corresponding ratchet-like pumping of calculated *j*(t); the bottom panel shows the comparison between simulated *Γ*-*T* profile (filled square) and experimentally measured *Γ*-*T* profile (empty circle); and the inset shows the simultaneous mean trajectory of channel's reaction coordinate obtained during the simulation of corresponding *Γ*-*T* profile, with the first cycle marked by arrows. C^* function used is shown in Figure S13. Other parameters used are shown in Table 1 of the main paper.

© 2007 Nature Publishing Group

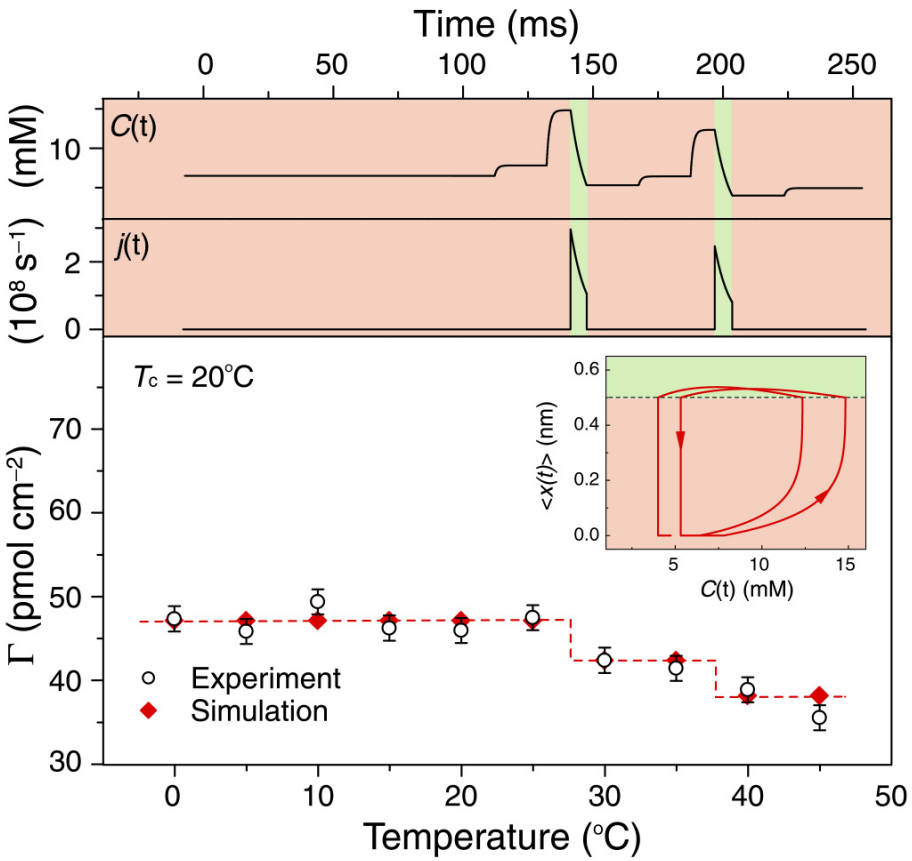

Supplementary Figure S4. Simulation of *Γ*-*T* profile of T_c = 20 ˚C, with compared to experiment. Below T_c = 20˚C the *Γ*-*T* profile should be sustained at a constant level, as observed experimentally, because after the ADNC is closed at T_c = 20˚C the PDC monolayer cannot store more thionine molecules and the maximum thionine quantity stored in the PDC monolayer is controlled by the *Γ*-*T* profile of the open state ADNC (Fig. 1d in the main paper, control, black line). The upper panel shows the calculated time evolution of *C*(t) corresponding to the simulation of *Γ*-*T* profile; the middle panel shows the corresponding ratchet-like pumping of calculated *j*(t); the bottom panel shows the comparison between simulated *Γ*-*T* profile (filled square) and experimentally measured *Γ*-*T* profile (empty circle); and the inset shows the simultaneous mean trajectory of channel's reaction coordinate obtained during the simulation of corresponding *Γ*-*T* profile, with the first cycle marked by arrows. C^* function used is shown in Figure S13. Other parameters used are shown in Table 1 of the main paper.

© 2007 Nature Publishing Group

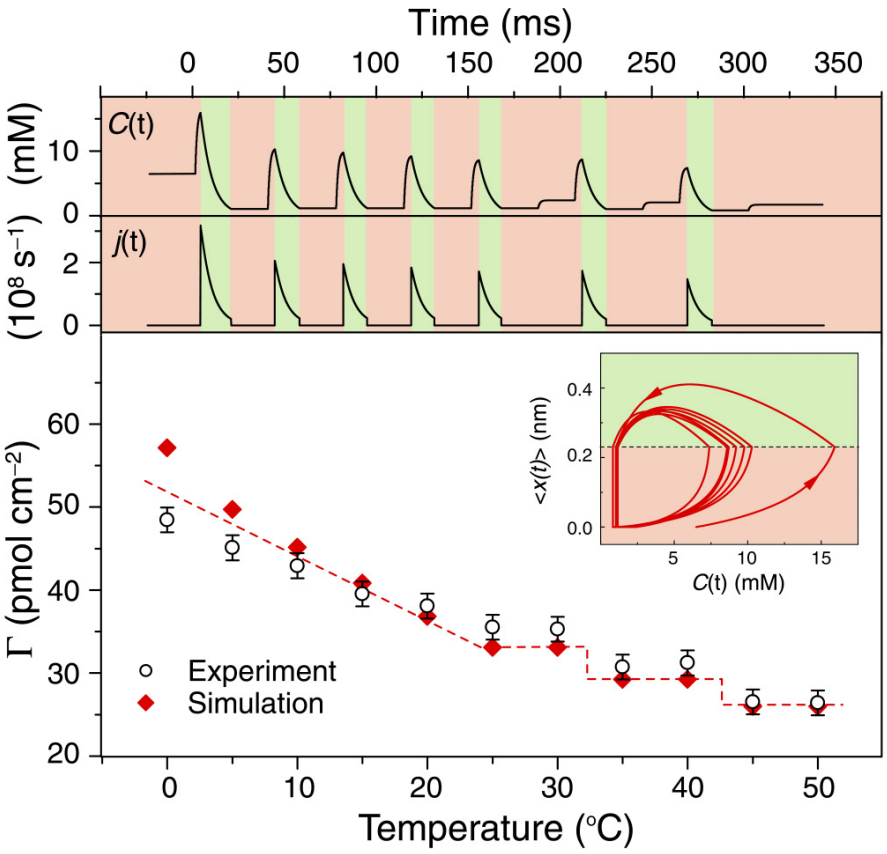

Supplementary Figure S5. The mixed behavior of one crossover at $T = T^*$ (≈ 25 °C), giving $C^* < C_{max}$ at $T < T^*$ (as demonstrated by red dashed line in Fig. 3 of the main paper). The upper panel shows the calculated time evolution of $C(t)$ corresponding to the simulation of Γ-T profile; the middle panel shows the corresponding ratchet-like pumping of calculated $j(t)$; the bottom panel shows the comparison between simulated Γ-T profile (filled square) and experimentally measured Γ-T profile (empty circle); and the inset shows the simultaneous mean trajectory of channel's reaction coordinate obtained during the simulation of corresponding Γ-T profile, with the first cycle marked by arrows. C^* function used is shown in Figure S13. Other parameters used are shown in Table 1 of the main paper.

© 2007 Nature Publishing Group

Supplementary Note

Note S1. Three key time scales

Our analysis for the stochastic motion of both DNA channels and solute particles (thionine) involves three key time scales, which are necessary to take all possible factors into a unified physical picture. They are (*i*) gating times of DNA channels (τ_g), (*ii*) transport times of solute particles through DNA channels (τ_t), and (*iii*) collision times of either inter-particle or channel-particle (τ_c). A simple analysis shows $\tau_g \gg \tau_t > \tau_c$ as described as follows. thionine's diffusion coefficient is $D_t \approx 10^{-8}$ m^2/s, and channel length is $L \approx 5$ nm, giving $\tau_t \approx L^2/D_t \approx 2.5$ ns. Conformational diffusion coefficient of single DNA channels is $D \approx 10^{-13}$ m^2/s, and channel radius variation during gating is $\Delta R \approx 0.5$ nm, giving gating times $\tau_g \approx \Delta R^2/D \approx 2.5$ μs$\gg \tau_t$. Typical channel-particle and interparticle spacing is $\lambda \sim 5$ Å, and ambient thermal velocities is $v_T \approx 4 \times 10^4$ cm/s, giving collision times $\tau_c \approx \lambda/v_T \approx 1$ ps $< \tau_t$.

The dilation or shrinkage of DNA channels is much slower than the thionine transport across the channel ($\tau_g \gg \tau_t$), which means that relaxation time of transport current excitation (or quenching) during the opening (or closing) of the channels can be neglected on the time scale of τ_g. On the other hand, one complete transport process of single particle involves many times of collision events ($\tau_t > \tau_c$), indicating that a quasi-constant mean stress, p, of single particle acts on the inner surface of the channel, which is averaged out within observation times between τ_t and τ_g. These time scales establish microscopic thermodynamic conditions for the channel-particle interaction system studied herein.

Note S2. Energy landscape of DNA channels

S2.1 The flexibility of DNA channels

The flexibility of the DNA channels formed by dsDNA membranes is different from protein channels embedded in lipid bilayer membranes[1–4]. Protein channels are formed by tight binding (short-range interaction) between subunits, which do not allow a remarkable stochastic motion between subunits. The protein channel usually allows no more than 1 Å stochastic displacement around its equilibrium position[5]. However, a DNA channel is formed from the neighboring dsDNA molecules whose interactions are the screened electrostatic interaction (long-range interaction) that is weak enough to allow them to move stochastically relative to each other, usually ~1 nm stochastic displacement[6–9]. The flexibility may be considered the origin of the nonequilibrium gating of the DNA channels.

The mechanical sensitivity of a nanochannel may arise from two aspects. One comes from the applied forces outside the channel. For example, in the case of membrane protein channels, the force gating the channel is usually originated from the geometrical deformation of the membrane because of the flexibility of the lipid bilayer membrane, which constitutes an important mechanism of mechanical gating of protein channel[4,10,11]. The other comes from the applied force inside the channel, which can be originated from the solute particles transporting though the channel. In the past studies, this effect is usually ignored because it is likely not important for protein channels. However, the DNA channels formed by dsDNA membranes on solid surface are hard to receive spontaneous tension from the dsDNA membrane deformation outside the channel that is able to gate the channel because the dsDNA membrane's shape is fixed by the solid

© 2007 Nature Publishing Group

substrate on which it attached. Thus, the second aspect dominates the gating mechanism of DNA channels. This difference makes the DNA channel's gating can not be described by the gating mechanisms of the mechanosensitive protein channels.

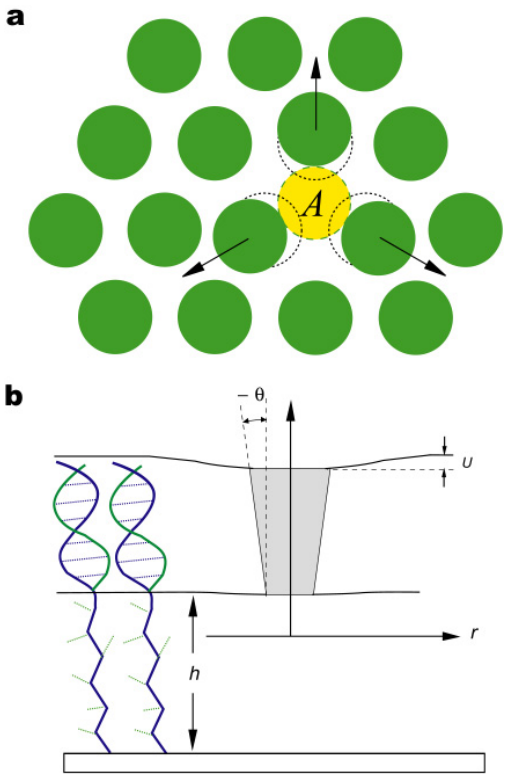

Supplementary Figure S6. Schematic drawing of DNA channels deformation. (**a**) Top view of a DNA channel that is dilated. Each green circle represents a dsDNA molecule. (**b**) Side view of the DNA channel and its membrane. The decline mismatch *U* is the difference between the channel thickness and the equilibrium DNA membrane thickness. We assume the surface of DNA membrane is normal to the orientation of DNA channel.

S2.2 Free energy for DNA channel deformation

The DNA channels formed in two-dimensional columnar assembly of dsDNA molecules, typically shown in Fig. S6a, have a complex conformational landscape, which depends on a large number of microscopic degrees of freedom that are analytically intractable. Although one could solve a precise conformational landscape by classical molecular dynamics, this does not help to answer the problem of this study. We need to find a minimal model that captures the main characteristics of the DNA channels, based on which we can show numerical coupling of channel gating with transport flux pumping. We consider that the Gibbs free energy of one DNA channel comprises three coarse-grained contributions: (1) the elastic energy between the dsDNA molecules that form the channel, which can be written as $\frac{1}{2}B(R-R_0)^2$, where R is the radius of the DNA channel, R_0 is the channel radius at original closed (equilibrium) state, and B is the elastic modulus; (2) the potential caused by line tension along the edge of the channel, $f'L$, where f' is line tension, and L is the circumference of the channel; (3) the potential caused by area tension across the in-plane area of the channel, γA, where γ is the area tension, and A is the in-plane area. Therefore, the Gibbs free energy describing the deformation of the DNA channel is

$$G=\frac{1}{2}B(R-R_0)^2+f'L+\gamma A+G_0' \qquad \text{(S1)}$$

where G'_0 is the absolute free energy when we remove all the three contributions.

The elastic modulus in the first item of equation (S1) has two contributions. One comes from the intermolecular interaction. The other comes from the ssDNA spcers, which act like a

© 2007 Nature Publishing Group

pendulum in solution. Both of the contributions approximate the Hooke's law at second order. The former part can be asymptotically calculated from Kornyshev-Leikin theory[6-8] for DNA interactions using $B_1 = b\frac{\partial^2 U_{KL}(R=R_0)}{\partial R^2}$, where b is a structure factor that can be determined from the geometry of the channel. For a channel formed by three duplexes with hexagonal packing order, $b = \sqrt{3}/2$. The dsDNA membrane is in an electric field E originating from the repulsion of dsDNA membrane surface against the gold surface. This part can be estimated by $B_2 = \sqrt{\frac{2\sigma E}{h}}$, where σ is the mean charge of each dsDNA molecule, and h is the height of the reservoir in the ADNC, i.e., the contour length of ssDNA skeleton.

The line tension in the second item of equation (S1) is positive when the DNA channel is dilated. It also consists of two dominant contributions, thickness deformation and spontaneous curvature. The thickness deformation is induced by the conformational incline relative to the normal direction of the membrane surface. The thickness deformation energy is $G_1 = f_U \cdot 2\pi R = (1/2)\, KU^2 \cdot \pi R$, where K is an effective elastic modulus and is independent of DNA length, and U is half the conformational incline as defined in Fig. S3b (ref. 10). The area of the part of the DNA membrane that is deformed by channel dilation is roughly equal to the circumference of the channel times an elastic decay length. The free energy induced by spontaneous curvature comes from the locally increasing the curvature stress generated by DNA columnar packing along its self-assembly plane. The radial dependence of this free energy is linear, because the effect is localized around the channel. Because the two sides of the dsDNA membrane in the real cases are asymmetric, with one side linked to solid surface, the spontaneous curvature of the top and bottom leaflets $C_{\pm}$ can be very different. It can work in terms of the composite spontaneous curvature of membrane near the channel, $C \equiv (1/2)\,(C_+ - C_-)$. The contribution of the deformation energy induced by spontaneous curvature is given by $G_2 = f_C \cdot 2\pi R = K_B C H' \cdot 2\pi R$, where H' is the mid-plane slope and K_B is the bending modulus, which roughly scales as the third power of the membrane thickness[10].

The area tension in the third item of equation (S1) arises from the repulsive tendency of the DNA molecules surrounding the channel. When the channel is dilated, it causes the compression of the two-dimensional packing of the surrounding DNA molecules. This effect makes the area tension positive as the form written in equation (S1).

After the rearrangement of these items, the Gibbs free energy of DNA channel deformation can be written explicitly in terms of the channel radius as

$$G(R) = \alpha \cdot \pi R^2 - f \cdot 2\pi R + G_0 \qquad \text{(S2)}$$

where $\alpha = B/2\pi + \gamma$, $f = BR_0/(2\pi) - f'$, and $G_0 = G_0' + \frac{1}{2} BR_0^2$. A free channel corresponds to the minimum energy of $G(R_0) = G_0 - \pi f^2/\alpha$ with $R_0 = f/\alpha$. Similar representation recently has been used to analyze the gating of protein channels[10,11]. However, the area tensions and line tensions in our case and in the case of protein channels have different sign. Although this model is coarse-graining and approximate the real case, in which we ignore many degrees of freedom that are less important, it can help with a theory working analytically or numerically.

© 2007 **Nature Publishing Group**

Note S3. Conformational stochastic dynamics of DNA channels

In previous Section, we have established a coarse-graining model that can represent the energy of channel's deformation as a function of channel's radius. This representation simplifies the dynamic analysis of channel gating under external perturbation. Mechanosensitive protein channels usually adopt bistable conformational deformation energy[10–12]. Although its open state is triggered by external mechanical perturbation, the open state is usually not considered sensitive to the pressure exerted by transporter particles because the gating may be understood as a conformational diffusion from one local minimum to another local minimum. DNA channels in our model system have different characteristics, whose gating is merely sensitive to mechanical interactions between channels and permeating particles. These interactions could contribute more non-equilibrium effects on the channel gating. The conformational stochastic dynamics between the open and closed states of a DNA channel can be described in terms of a one-dimensional reaction coordinate dynamics $x(t) = R - R_0$ in the conformational potential $G(R)$. Consider that the collision of thionine molecules with the inner surface of the channel generates stress, $F(t)$, on the inner surface of the channel along the coordinate $R(t)$, which is defined as the mean force averaged out within observation times much larger than mean transport times (τ_t). The corresponding Fokker-Plank equation (FPE) for the probability density function (PDF) describing the channel dynamics under the external force $F(t)$ reads[12,13]

$$\frac{\partial p(x,t)}{\partial t} = D\frac{\partial}{\partial x}\left(\frac{\partial}{\partial x} + \beta\frac{\partial}{\partial x}[G(x+R_0) + F(t)x]\right)p(x,t), \tag{S3}$$

where $p(x,t)$ is probability density of the reaction coordinate at $(x, x + dx)$, D is the conformational diffusion coefficient. Inserting Smoluchowski approximation[13] $p(x,t) = \sqrt{\alpha\beta}\exp\left[-\pi\alpha\beta(x - \langle x(t)\rangle)^2\right]$ into equation (S3), one can easily derive equation (1) of the main paper. The exact solution of the equation with initial condition of $\langle x(0)\rangle = 0$ is $\langle x(t)\rangle = \beta D e^{-2\pi\alpha\beta Dt}\int_0^t e^{-2\pi\alpha\beta Dt'}F(t')dt'$.

Unlike the bistability nature of protein ion-channel gating[10–12], the DNA channels in this study show no bistability. A free channel corresponds to the closed states, which represents a stable state. Only when the channel dilates under the stress from the solute particles inside the channel to reach a critical radius, the channel is permeable to the particles studied. The so-called open state of the DNA channel does not correspond to any local minimum in the free energy landscape. It is in an unstable state far away from the minimum of the energy landscape, thus, far away from equilibrium. We may conclude that the flexible channel like this case is only gated in non-equilibrium states. These special features make the transport flux through the channel to behave like "ratchet" pumping. Our calculations shown in Fig. 2c-e of the main paper actually describe in detail one cycle of such "ratchet" pumping process.

Note S4. Single-file nature of the transport through DNA channels

S4.1 Channel parameters

The channel parameters include channel radius, channel length, and geometrical shape. The channel radius can be determined from the DNA density in the dsDNA membrane. In previous studies, the DNA density on gold surface are in the range (6~12) × 10^{12} molecules·cm^{-2} (refs. 14,15). Atomic force microscopy studies have shown that dsDNA molecules in dense dsDNA

© 2007 Nature Publishing Group

membrane with complete coverage orient perpendicular to gold surface[15–17]. Thus it is conceivable that the dsDNAs are juxtaposed in parallel. If the duplexes are in ideal parallel, the length of a channel approximates the length of dsDNA molecules. In this study, the dsDNA is 15 bp, equivalent to about 5 nm. The geometry of the channel is related to the way that dsDNA packing. Assume that dsDNA can pack into regular manner in local area, as supported by experiments[15,18]. In hexagonal lattice, a channel is formed by three nearest neighboring dsDNA helices. The distance between nearest neighboring molecules is dependent of the ionic strength of the buffer solution, which can screen the long-range electrostatic interaction between the dsDNAs[6–8]. Both theory and experiments show the distance to be a = 2.5~3.5 nm. The channel diameter is $2(a/\sqrt{3} - 1)$, giving 0.9~2 nm. In square lattice, a channel is formed by four dsDNA helices. The channel diameter is $(\sqrt{2}\,a - 2)$, giving 1.5~2.9 nm. Because the diameter of thionine is about 0.8 nm and its electrostatic repulsion distance with dsDNA is around 0.5 nm, a channel diameter less than $2 \times 0.8 + 3 \times 0.5 = 3.1$ nm will give a precise single-file pore. The single-file behavior is still accurate even for channel diameters ~(2–3) × particle diameters since overtaking requires a restricted subset of geometries and will be statistically rare[19]. Thus, a channel diameter less than $4 \times 0.8 + 5 \times 0.5 = 5.7$ nm should give a good approximate single-file pore. In the defects, a channel is still likely formed by five or more dsDNA helices. However, if there are pores among dsDNA membrane large enough to allow thionine permeation anytime, they should play no role in channel gating, and do not contribute to the stepwise effect of the Γ-T profiles. Moreover, in our previous work, we have evaluated the defects that allow thionine to permeate through the dsDNA membrane at the closed state of the ADNC[15,20], showing that their effect as a whole is on the level of noise if the dsDNA membrane is well self-assembled. Experimentally, its contribution in Γ-T profile is always like the off state curve. Theoretically, since thionine transport through it in any condition, this case gives trivial behavior of transport and also no corresponding channel gating problem. Thus it is not interested in this study.

S4.2 Single-file diffusion

Although we have discussed in the previous section the experimental indication of the single-file transport especially concerning the channel parameters, we would like extend the discussion to solute particles. The single-file nature of particle transport through the DNA channels originates from the limited space inside channel with respect to the particle size. The diameter of cross section inside the DNA channel is about 0.5 ~ 1.5 nm. In our experiments the thionine molecules are ~1.1 nm in size (Fig. S7). Thus, the particles can merely transport through the opened DNA channel in a single-file fashion.

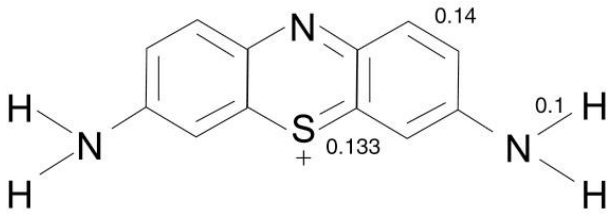

Supplementary Figure S7. The physical size of thionine. The numbers label the covalent bond length with unit of nm. The size is estimated as: $\sqrt{3} \times (0.133 + 3 \times 0.14 + 0.1) \approx 1.13$ nm.

© 2007 Nature Publishing Group

Single-file transport refers to the one-dimensional motion of interacting particles in channels which are so narrow that the mutual passage of particles is excluded[21–25]. Thus the motion of individual particles requires the collective motion of many other particles in the same direction. This restriction leads to an anomalous behavior of the self-diffusion for overdamped systems in the longtime limit[21–25]. In other words, the mean-square displacement $\langle y^2(t)\rangle$ of a tracer particle for t much larger than the direct interaction time τ (i.e., the time that a particle needs to move a significant fraction of the mean particle distance) is given by $\lim_{t\gg\tau}\left\langle y^2(t)\right\rangle = 2F\sqrt{t}$, where F is the single-file diffusion mobility. In the short-time regime ($t < \tau$ or $t \sim \tau$), the single-file diffusion was observed obeying normal behavior, i.e., $\langle y^2(t)\rangle = 2D_0t$, where D_0 is the one-dimensional self-diffusion coefficient[25].

S4.3 Steady-state flux

In this study, the DNA channels are so short that the diffusion time across the channel is comparable to τ. The anomalous diffusion behavior can be safely ruled out from this study. As a result, the mean field approximation used in describing the Langevin dynamics of particles transporting the channel is appropriate as supported by related studies[26-28]. The potential $U(y)$ of mean field includes both the exclusion interactions between particles and the potential applied on the particles along the channel because of either electrostatic fields or molecular polar interactions between particles and channels.

Brownian motion of solute particles along a narrow channel is in the overdamped limit of one-dimensional Langevin dynamics, described by the equation $\gamma\dot{y} = -U'(y) + \xi(t)$, where $U(y)$ is the potential of mean field that guides the transport of particle through the channel, $\xi(t)$ is a Gaussian white noise with $\langle\xi(t)\rangle = 0$ and $\langle\xi(t)\,\xi(0)\rangle = 2D_p\gamma^2\delta(t)$. Here, $\delta(t)$ is the Dirac-delta function; D_p is the effective diffusion coefficient of a solute particle inside the channel, which is related to γ through Einstein relation $D_p = k_BT/\gamma$ according to the fluctuation-dissipation theorem. The corresponding Fokker-Plank equation of the dynamics reads

$$\begin{aligned}\partial_t p(y,t) &= -\partial_x j(y,t),\\ j(y,t) &= -\frac{1}{\gamma}[\varepsilon\partial_x p(y,t) - U'(y)p(y,t)],\end{aligned} \tag{S4}$$

where $p(y,t)dy$ is the probability of finding a solute particle in $(y, y + dy)$ along the channel, $j(y,t)$ is the local, instantaneous flux of particles through the channel, γ is the friction coefficient, and $\varepsilon = k_BT/m$, and m is the particle mass. In the steady state, the flux is constant throughout the channel ($\partial_t p(y,t) = -\partial_y j(y,t) = 0$), we have

$$\begin{aligned}j(t) &= A_1C(t) - A_2C_2\\ A_i &= \frac{\varepsilon}{\gamma}e^{U_i/\varepsilon}\left[\int_{y_1}^{y_2} e^{U(y)/\varepsilon}dx\right]^{-1}, \quad i = 1,2\end{aligned} \tag{S5}$$

where $C(t)$ is the concentration of solute particles in the internal reservoirs of the DNA nanocompartment, C_2 is the concentration in the external bath that maintains constant. The detailed mathematical approaches to equations (S4) and (S5), as well as their physical reasonability, were clearly described in ref. (26).

© 2007 **Nature Publishing Group**

Note S5. Simulation on mean residence number of thionine inside a channel

S5.1 One-dimensional lattice exclusion model

Before we can couple the channel gating with single-file transportation, the microscopic dual criticality should be related to macroscopic quantity. This problem is equivalent to that how the different concentration gradients provide microscopic external force on the channel. The first step towards the solution is to clarify how many particles inside the channel at a time at given concentration gradient. Due to the single-file nature of thionine transport across the DNA channels, we use a one-dimensional exclusion model to describe the single-file particle (thionine) flows[19,29]. Consider the nanochannel shown in Fig. S8, with solute particles driven from left (inner) to right (external) by osmotic pressure or by hydrostatic pressure. A single-file channel is divided into M sections labeled i, each of length $l \geq$ diameters of solute particles. The site of particle in the left reservoir is labeled $i = 0$, and that in the right reservoir is labeled $i = M + 1$. The occupation of particles at site i is defined by $\tau_i \in \{0, 1\}$. The probability in time dt that a particle enters the channel from the left reservoir is $P_{01}dt$ if site $i = 1$ is unoccupied. Similarly, the probability that a particle enter left reservoir from the channel in time dt is $P_{10}dt$. The entrance and exit probabilities for a particle in the right reservoir in time dt are similarly defined as $P_{M,M+1}dt$ and $P_{M+1,M}dt$. In the channel interior, solute particles move from site i to $i \pm 1$ with probability per unit time $P_{i,i\pm1}$ only if the adjacent site is unoccupied, $\tau_{i\pm1} = 0$. Under the approximation of a uniform and isotropic channel, $P_{i,i\pm1}$ may be simplified to P_c.

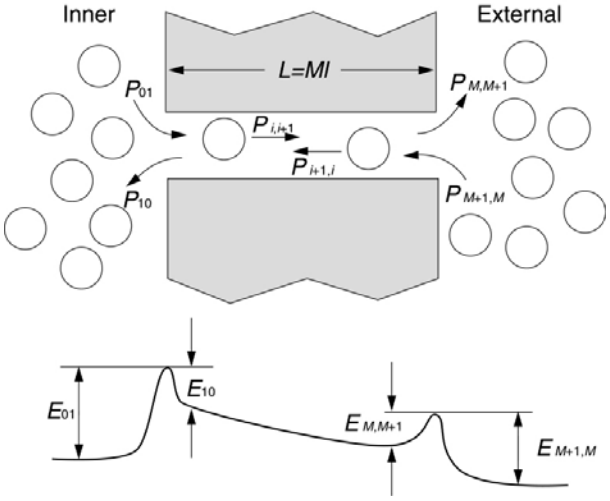

Supplementary Figure S8. Schematic drawing of osmosis and pressure driven flow through DNA channels separating inner reservoir of the ADNC and external infinite reservoir. The coefficients P_{01}, P_{10}, $P_{M,M+1}$, and $P_{M+1,M}$ are particle entrance and exit probabilities at channel ends. The coefficients $P_{i,i+1}$ and $P_{i+1,i}$ are hopping probabilities of particle along the one-dimensional channel. The bottom part of this figure depicts energy barriers for solute particles.

In Note S1, we have described microscopic thermodynamics in the channel-particle interaction system involves three time scales. For the simulation performed here, additional two time scales should be taken into account: the mean times that the absolute residence number of solute particles filled in the channel changes its value one time, defined as τ_n, and the times over which we average the accurately simulated residence number of particles in the channel interior,

© 2007 Nature Publishing Group

defined as τ_s. Considering that local thermodynamic equilibrium (LTE) is satisfied in the system, the relation among the time scales is $\tau_g > \tau_s \gg \tau_n > \tau_t > \tau_c$.

Based on LTE condition, the kinetic rates, P_{ij}, can be estimated from Arrhenius forms

$$P_c \approx \frac{v_T}{l} e^{-E_c/k_BT}$$

$$P_{01} \approx \frac{1}{4} C(t) v_T \pi r^2 e^{-E_{01}/k_BT}$$

$$P_{M+1,M} \approx \frac{1}{4} C_2 v_T \pi r^2 e^{-E_{M+1,M}/k_BT} \qquad \text{(S6)}$$

$$P_{10} \approx \frac{v_T}{l} e^{-E_{10}/k_BT}$$

$$P_{M,M+1} \approx \frac{v_T}{l} e^{-E_{M,M+1}/k_BT}$$

where $v_T = \sqrt{\frac{k_BT}{m}}$ is the thermal velocity, l is the length of a channel section, r is the channel radius, $C(t)$ is the particle concentration at the inner reservoir of the ADNC, C_2 is the particle concentration at external solution, E_c, E_{01}, E_{10}, $E_{M+1,M}$, and $E_{M,M+1}$ are activation energies for solute particle to realize the corresponding position variation. Since a highly flexible DNA channel can change its conformation in response to the change of the mean residence number ($\overline{n}$) of particles in the channel interior, all the kinetic rates and corresponding activation energies are the functions of $\overline{n}$.

S5.2 Simulation method

To simulate and calculate the statistical quantity of $\overline{n}$ as a function of concentration gradient ($C(t) - C_2$) applied on both sides of the channel, the first step is to count the number of microstates of the system and determine the transition probabilities between two adjacent states by the use of equation (S6). The microstates are represented as $\{\tau_i(t)\}$ ($\tau_i(t) \in \{0,1\}$, $i \in [1, M]$), where $\tau_i(t)$ is previously defined as the number of solute particle occupying the ith section of the channel. The instantaneous number flux between section i and i+1 is

$$j_i(t) = P_{i,i+1}\tau_i(t)[1 - \tau_{i+1}(t)] - P_{i+1,i}\tau_{i+1}(t)[1 - \tau_i(t)]. \qquad \text{(S7)}$$

Note that $j_i(t) \in \{0, \pm 1\}$. The following expression is used to measure $\overline{n}$ in computer simulation program

$$\overline{n} = \frac{1}{T}\sum_{t_0}^{t_0+T} n(t), \qquad \text{(S8)}$$

where t is dimensionless time, t_0 is the time when the measurement begins, $n(t)$ is the particle number occupying in the channel interior at time t, and T is the total time interval over which the measurement maintains.

The probabilities P_{ij} should change with the change of channel diameter when the channel is dilated by the particles filling in the channel. The change behavior can be understood according to

$$\frac{\partial P_{ij}}{\partial \overline{n}} \approx -\frac{v_T \beta}{l} e^{-\beta E_{ij}} \left(\frac{\partial E_{ij}}{\partial r}\right)\left(\frac{\partial r}{\partial \overline{n}}\right). \qquad \text{(S9)}$$

Since $\frac{\partial E_{ij}}{\partial r} < 0$ and $\frac{\partial r}{\partial \overline{n}} > 0$, $\frac{\partial P_{ij}}{\partial \overline{n}} > 0$. The probabilities used in our simulations are

© 2007 Nature Publishing Group

accordingly shown in Fig. S9. As a good approximation, the probability $P_{M,M+1}dt$ and $P_{M+1,M}dt$ are fixed on order of 10^{-8}, and independent of $\overline{n}$. Set t as the dimensionless simulation time. At t = 0, the temperature and concentrations are fixed at given values: T = 300 K, $C(0)$ = 10 mM, C_2 = 0.01 mM, and τ_i ($i \in [1,M]$) is set zero. Let solute particles to move randomly from one site to its adjacent site, weighted by corresponding transition probability, if the adjacent site is not occupied. We set τ_c = 1, then the time scale of n variation, τ_n, would be on the order of magnitude of $10^3 \sim 10^4$. Thus, the system will definitely achieve the equilibrium state and a stable distribution of particles after $t = 10^8$. After that, we measure the mean residence number in a time interval of $\tau_s = 10^9$, and collect the simulated data. If a large amount of simulated data is obtained under the same condition, we find that the data obey a Gaussian distribution without obvious deviation.

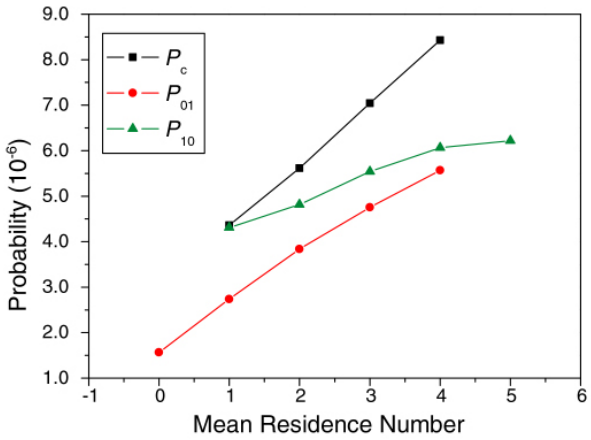

Supplementary Figure S9. The probabilities of entrance, exit, and hopping of particles as a function of the mean residence number, which are typically used in the simulation of Figs. S10 and S11.

S5.3 Results

The mean residence number $\overline{n}$ as a function of the concentration gradient is simulated, with temperature fixed at 300K. In the simulations, the concentration of solute particle in external solution is fixed at C_2 = 0.01 mM, whereas the concentration in ADNC ($C(t)$) varies from 0 to 20 mM. Figure S10 shows the typical simulation results for the cases of M = 4, 5, 6. The mean residence number under different concentration gradient can fit well to Langmuir isotherms. In Fig. S11, we further change the kinetic rates to test their effect on the simulations. It shows that the association constant in Langmuir isotherm does not change seriously in most cases. We observe that fluctuation in simulated data decrease seriously with increasing the entrance, exit, and hopping probabilities. In Figs. S11c, d, e, the simulated data fit fairly well to equation (S10) as shown below. The simulated Langmuir isotherms are well reasonable and theoretically expected. Actually, if LTE condition is well satisfied in a single-file channel system, the mean residence number should obey a single-site occupation mode, which mathematically is the same as single-site binding mode, i.e., first-order Langmuir isotherm. Using equilibrium statistical mechanics based on partition function weighted by binding energies of each site, one can exactly work out a first-order Langmuir isotherm relation between $\overline{n}$ and the concentration gradient $C = C(t) - C_2 \approx C(t)$, which is written as

© 2007 Nature Publishing Group

$$\overline{n} = \left(\frac{C}{C + \kappa^{-1}} \right) n_m , \tag{S10}$$

where κ is the association constant and n_m is the maximum mean residence number. And

$$\kappa^{-1} \propto \left(\frac{2\pi m}{\beta} \right)^{1/2} e^{-\beta \varepsilon_c} , \tag{S11}$$

where $\beta = 1/k_B T$, m is the particle mass, and ε_c is effective site occupation energy for a particle.

Our simulations imply an interesting conclusion: if measurement on $\overline{n}$ does not distinguish the difference between individual particles, the n averaging over a time interval that is wide enough on the steady-state flux of a one-dimensional nonequilibrium transport is equivalent to static occupation of equilibrium particles along the channel. One reason for this conclusion is that during the measurement of $\overline{n}$ -C isotherms, the roles of the left and right reservoirs are the same, so that their exchange of particle with channel can be treated as a whole, which results in that steady-state flux is equivalent to zero net exchange number between channel and the (left and right) reservoirs as a whole. This conclusion also shows the reasonability of applying an equilibrium statistical mechanical method on the mathematical derivation of $\overline{n}$ -C isotherms under LTE conditions. This can also explain why the changes of probabilities of entrance, exit, and hopping of particles relative to the channel do not seriously affect the simulated association constants.

We then go back to consider that the stress, $F(t)$, generated by collisions of thionine molecules with the inner surface of the channel. Given the single-file behavior as explained in Note S4 and $\tau_t > \tau_c$ as described in Note S1, $F(t)$ may be related to the mean residence number of the thionine molecules along the channel, $\overline{n}(t)$, by a linear form $F(t) = p \cdot \overline{n}(t)$, where p is the mean stress of single thionine acting on the inner surface of the channel. One then obtains equation (2) in the main paper, that is $F(t) \approx \dfrac{p n_m C(t)}{C(t) + \kappa^{-1}}$.

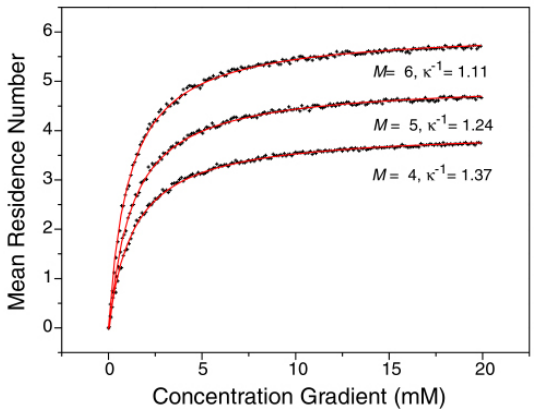

Supplementary Figure S10. The relation between the mean residence number and concentration gradient for three different lengths of the DNA channels. In the experimental system of DNA nanocompartment, specially designed dsDNAs have 15~20 base-pairs and a 6~7 nm double helix length. Comparing the channel length with the particle size, M = 5 typically reflects our experimental configuration. Red lines fit the data with equation (S10).

© 2007 Nature Publishing Group

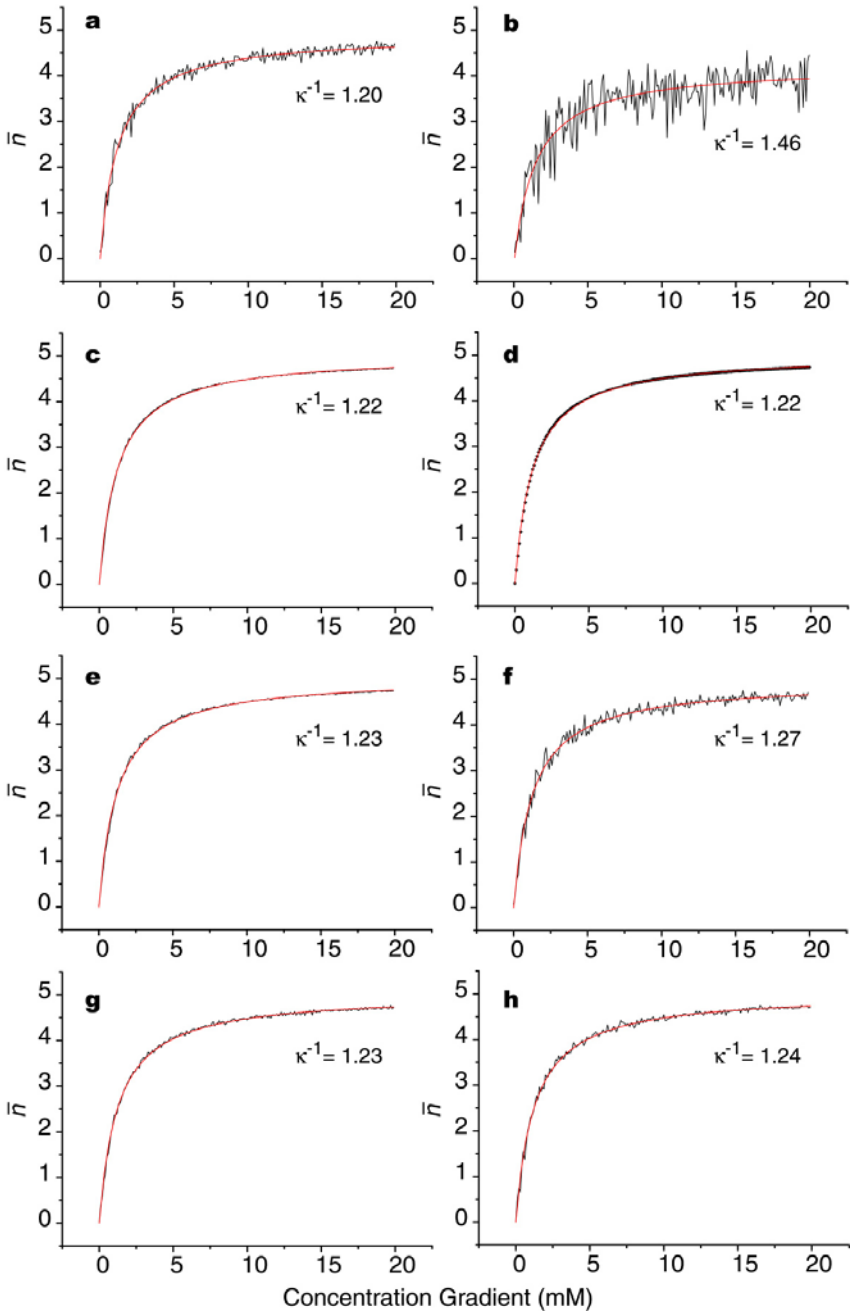

Supplementary Figure S11. The effect of the changes of probability on the simulated $\bar{n}$ -C relations. Unit of κ^{-1} shown is mM. The data simulated on all probabilities shown in Fig. S9 times a factor of (**a**) 0.1, (**b**) 0.01, (**c**) 10, (**d**) 100. (**e**) Only P_c times 10. (**f**) Only P_c times 0.1. (**g**) P_{01} and P_{10} times 10. (**h**) P_{01} and P_{10} times 0.1. Red lines fit the data with equation (S10).

© 2007 **Nature Publishing Group**

Note S6. Steep-wall potential and critical radius

The static channel-particle interactions can be simulated by a steep-wall potential[24]

$$\Phi_{CP}(\rho) = \begin{cases} 4\varepsilon\left[\left(\frac{\rho-\rho_0}{\sigma}\right)^{12} - \left(\frac{\rho-\rho_0}{\sigma}\right)^{6}\right] & \rho - \rho_0 > \sigma / \sqrt[6]{2} \\ 0 & \rho - \rho_0 \le \sigma / \sqrt[6]{2} \end{cases} \quad \text{(S12)}$$

where ρ is the distance between the axis of the channel and the center of the solute particle, and $\rho_0 = R - R^*$. According to equation (S12), one can evaluate $R^* = \sigma + r$, where r is the radius of solute particles. We are aware that this potential is not exact. However, it was shown that simulation based on this potential can produce results agreeing with experimental observation of single-file diffusion across nanochannels in molecular sieves[24].

The critical radius R^* describes the critical behavior of the channel's conformational transition between the insulating and conducting states relative to the solute particles of interest. One would expect that this transition is first-order, thus casting a physical parameter to reflect the discontinuity. Obviously, the parameter is transport flux as a function of channel radius, since the channel's conformational changes can be described as a function of R (as explained in Note S2). Of current experimental techniques, there is a lack of the approaches to simultaneously measure the channel radius changes and transport flux through the single channel. In our entire analysis, we have statistically assumed that all channels share the same geometry. Thus the R^* used in our analysis is experimentally the mean from different channel geometry. The geometrical diversity of the channels in a real DNA membrane should share the same statistical behavior, since the main feature length of the geometry are identical. Similar arguments are available to our understanding to the critical forces (F_c, F_o) and critical concentrations (C_c, C_o), as well as the gating threshold (F^*, C^*). For example, note that in Fig. 2c-e of the main paper the trajectory of DNA channel conformation is the mean value over a large number of individual trajectories. A single trajectory without average treatment contains stochasticity originated from Gaussian noise and system fluctuation. Thus, a single real trajectory of DNA channel can result in different critical concentrations. The critical concentrations determined in the mean trajectories of DNA channels should be understood as mean critical concentrations averaged over a large number of individual trajectories. If we have experimental method to measure the critical concentrations of single trajectory of single DNA channel, the measured data should have indispensable fluctuation consistent with stochastic factors in Fokker-Plank equations.

Note S7. Numerical calculation procedure of the complete flux-coupled gating trajectories

The general calculation method used to couple the gating of flexible DNA nanochannel with single-file transport flux of solute particles, as shown in Figs. 2c-e and Fig. 4 of the main paper, is summarized as following procedures:

Step 1: to estimate the critical radius of the channel gating from the channel radius and particle sizes. In the calculation of Figs. 2c-e in the main paper, the critical radius of the channel gating is estimated $R^* = R_0 + 0.3$ nm.

Step 2: to find the increasing phase of the concentration gradient across the channel. In the calculation of Figs. 2c-e in the main paper, the increasing phase of the concentration gradient is dominated by $C(t) = C_m(1 - e^{-t/\tau}) + C_1$.

© 2007 Nature Publishing Group

Step 3: to determine the opening critical concentration according to critical radius by solving the mean trajectory of the DNA channel dynamics (equation (1) in the main paper) corresponding to the increasing phase of the concentration. In the calculation of Figs. 2c-e in the main paper, the increasing phase of the concentration gradient is dominated by $C(t) = C_m(1 - e^{-t/\tau}) + C_1$. Using equation (1) in the main paper, the time evolution of $F(t)$ can be determined by $C(t) = C_m(1 - e^{-t/\tau}) + C_1$. Substituting the $F(t)$ in equation (1) of the main paper with the equation (2), the mean trajectory of the DNA channel represented by $\langle x \rangle$-C curve (Fig. 2e in the main paper) can be computed and the opening critical concentration C_o can be obtained from the curve to be C_o = 16.22 mM.

Step 4: to find the decreasing phase of the concentration gradient across the channel. As the opening of the channels, the kinetic behavior of $C(t)$ is dominated by equation (7) in the main text. To obtain an intuitive analysis, it is simple but instructive to select $N(t) = N_0$. After rearrangement of equation (7) in the main paper, the equation is simplified as $C(t) = \frac{C_m\tau_j}{\tau-\tau_j} e^{-t/\tau} + (C_o - C' - \frac{C_m\tau_j}{\tau-\tau_j} e^{-t_o/\tau}) e^{-(t-t_o)/\tau_j} + C'$, where $\tau_j = V(A_1N_0)^{-1}$, and $C' = A_2C_2 A_1^{-1}$.

Step 5: to determine the closing critical concentration gradient according to critical radius by solving the mean trajectory of the DNA nanochannel dynamics (equation (1) in the main paper) corresponding to the decreasing phase of the concentration gradient. Similar to the description in the *Step 3*, using the solution of $C(t)$ given in *Step 4*, we can determine the closing critical concentration C_c = 0.77 mM, by inserting equation (7) to equation (2), then inserting equation (2) into equation (1) in the main paper.

In the numerical calculation, we ignore some intrinsic complexity that is not important for the points studied here. First, we do not take into account the defects as their affection is not important to the macroscopic effects. In a real surface of DNA nanocompartment device, random microstructure or even nanostructure may contribute specific effect. Experiments showed that this effect is on the continuous small decrease of measured $C(t)$, which does not affect the pumping effect during the Γ-T profiling. Second, the microscopic behavior of molecules inside ADNC may be very different from those in the bulk solution. We do not take into account this effect because this deficiency does not affect the major character of the gating mechanism studied in this work, and also does not contribute specific effect on experiments. Third, in the steady state, $N(t)$ does not explicitly depend on $C(t)$, but has a constraint of $\sum_{i=0}^{N(t)} \pi(R_i^2 - R_0^2) \le \ell h$, where R_i is the radius of the ith open channel, ℓ is the circumference of the ADNC, and h is the effective height of the inner reservoir of ADNC. We used $N(t) = N_0$ in our calculation which is understood as the average value of $N(t)$ over the interval $t_o < t < t_c$. However, since the change of $N(t)$ over the interval $t_o < t < t_c$ is less dominant, this treatment is a good approximation to the real case.

This numerical calculation can be more precise by using more accurate $C(t)$ and $N(t)$ functions, which can make the discontinuity of first-order derivative of $C(t)$, $j(t)$, and $\langle x(t) \rangle$ vs. $C(t)$ to become continuous at critical points. Typically, $N(t)$ can be refined by using the probability of channel opening, $P_o = (1 + \exp(-\beta\Delta G))^{-1}$, where ΔG is the change of deformation energy during the channel opening[11]. However, the main features will not change under these detailed improvements. While available experimental techniques are far away from observation on the detailed dynamics, we do not work much further on these improvements. Theoretically, these

© 2007 **Nature Publishing Group**

improvements cannot essentially promote the quality of this study.

Note S8. Simulation methods of *Γ*-*T* profiles

Equation (1) in the main paper gives a threshold force $F^* = 2\pi\alpha(R^* - R_0)$ at a steady state ($\partial\langle x(t)\rangle/\partial t = 0$). The work of $F(t)$ can gate the DNA channels only if the maximum of $F(t)$ is larger than F^*. Substituting $F^* = 2\pi\alpha(R^* - R_0)$ into equation (2) in the main paper, one can immediately derive the equation (3) in the main paper, which provides a criterion of channel gating: the channels can be opened only if C_{max} is larger than C^*, where C_{max} is the maximum value of $C(t)$ after the increase of temperature triggers the thionine's release from PDC monolayer.

While in Note S7 we have descried how to numerically compute the $C(t)$ changes coupled with the channel motion trajectories $\langle x(t)\rangle$, the simulation of *Γ*-*T* profiles is to calculate the detailed trajectories of the channel motion coupled with $C(t)$ and $j(t)$ in every measurement step after the temperature change triggers the thionine release from PDC monolayer, where the channel opening events are determined by whether the C_{max} in such a measurement step could overwhelm C^*. Thus, besides the numerical method described above, the first step to simulate *Γ*-*T* profiles is the determination of C^* as a function of temperature.

S8.1 Determination of C^* as a function of DNA density and temperature

Equation (3) in the main paper suggests that the determination of C^* as a function of temperature is dependent of $\alpha(T)$ and $\kappa^{-1}(T)$, whereas other parameters are independent of temperature. The temperature dependence of $\kappa^{-1}(T)$ has been given in equation (S11). In the temperature of interest, it changes in a very small range and is nearly a constant. Here we first analyze α, then go to R_0.

It is intuitive that α is directly dependent of dsDNA density (ρ). The higher the dsDNA density, the larger the α. Assume that ρ_{max} is the high limit of ρ when the intermolecular spacing is absolutely equal to the dsDNA diameter. Of course, $\rho_{\max}$ is physically impossible, but can be approached infinitely by compression the dsDNA density with an infinite force, assuming that dsDNA helices are infinitely rigid. We notice that α should be divergent when ρ approaches $\rho_{\max}$ infinitely, that is, $\rho = \rho_{\max}$ gives a singularity of α as a functions of ρ. One may write down the asymptotic behavior of α near $\rho = \rho_{\max}$ as $\dfrac{k_\alpha}{(\rho_{\max} - \rho)^\lambda}$, where k_α and λ ($k_\alpha > 0$, $\lambda > 0$) are constants defining the behavior. On the other hand, when ρ decreases to a regime ($\rho < \rho_{\min}$) that allows interaction between neighboring dsDNA molecules to be negligible, the corresponding α should be zero. Here $\rho_{\min}$ measures the low limit of ρ that gives rise to non-zero α. Then, one obtain the behavior of α as

$$\alpha(\rho) = \begin{cases} \dfrac{k_\alpha}{(\rho_{\max} - \rho)^\lambda} & (\rho \to \rho_{\max}) \\ 0 & (\rho \le \rho_{\min}) \end{cases}, \tag{S13}$$

In light of this analysis, we can qualitatively plot the relation between α and ρ as shown in Fig. S12(a). Based on the above analysis, one should notice that ρ is dependent of temperature because the melting of dsDNA begins at a temperature much lower than the melting point. Although at such a temperature, the melted percent of dsDNA is rather small, the corresponding small decrease of ρ can result in large decease of α according to equation (S13) and Fig. S12. This is why we have to take into account the temperature dependence of α. The temperature

© 2007 Nature Publishing Group

dependence of ρ is proportional to the percent of non-melted dsDNA molecules, thus can be empirically fitted with a Boltzmann function

$$\rho = \frac{\rho_0}{1+e^{\Delta H/RT-\Delta S/R}}, \tag{S14}$$

where ρ_0 is the density of ssDNA immobilized on surfaces, ΔH and ΔS are the enthalpy and entropy differences of the dsDNA melting respectively. Equations (S13) and (S14) provide an understanding to the temperature dependence of α. According to equation (3) of the main paper, the temperature dependence of C^* is finally determined.

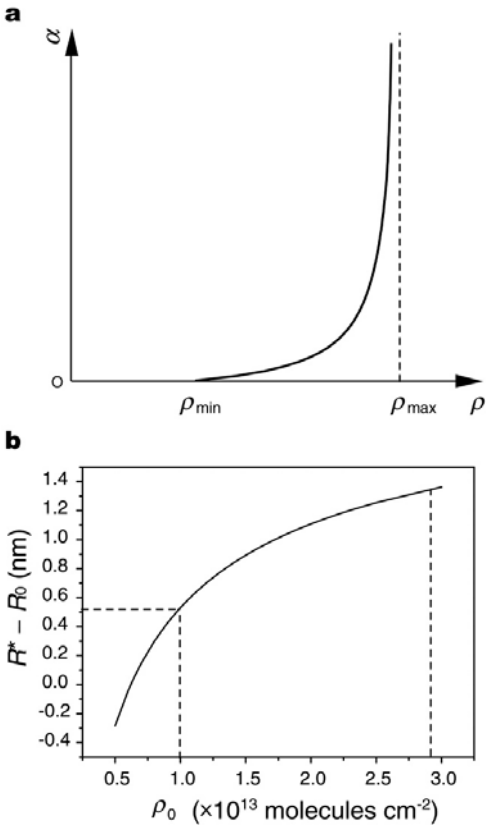

Supplementary Figure S12. (**a**) Schematic drawing on the relation of between α and dsDNA density. In our experiments, $\rho_{min} \approx 1.0 \times 10^{12}$ molecule·cm^{-2}, and $\rho_{max} \approx 2.9 \times 10^{13}$ molecule·cm^{-2}. (**b**) $R^* - R_0$ as a function of ssDNA density (ρ_0). A small variation of ρ_0 in the range of $(0.6 - 1.0) \times 10^{13}$ molecule·cm^{-2} gives rise to the change of $R^* - R_0$ in the range of 0 – 0.5 nm.

We then discuss the DNA density dependence of C^*. According to equation (3) in the main paper, the dependence arises from α and R_0. Whereas the relation between α and DNA density has been clarified by equations (S13), (S14), the relation between R_0 and DNA density appears simple. The relation in the case of hexagonal packing of dsDNA membrane is

$$R_0 = \sqrt{\frac{2}{3\sqrt{3}\rho_0}} - 1 \ \text{(nm)}. \tag{S15}$$

Note that we use the character ρ_0 to distinguish the ssDNA density from dsDNA density (ρ); the ssDNA density is independent of temperature. Figure S12(b) depicts the $R^* - R_0$ as a function of ρ_0. One may question why not consider R_0 as a function of ρ. We emphasize that for a well formed DNA channel, a slightly melting of its surrounding dsDNA molecules should have much less effect on R_0 because R_0 is inherently determined by the lateral interaction potential between neighboring dsDNA forming the channel. Although ρ is dependent of temperature, our modeling is merely correct at a temperature regime that allows a very small fraction of melting DNA, because substantial melting should lead to the breakdown of ADNCs and DNA channel. In our

© 2007 Nature Publishing Group

simulation of Γ-T profiles in the temperature regime of interest (0–50 ˚C), it is reasonable to consider the effects of temperature and ρ_0 as two independent factors. Combing equations (S13)-(S15) with equation (3) of the main paper, one can make clear the DNA density dependence of C^*. These analyses establish a basis for the simulations of Γ-T profiles. Figure S13 summarizes the temperature-dependence of C^* used in the practical simulations.

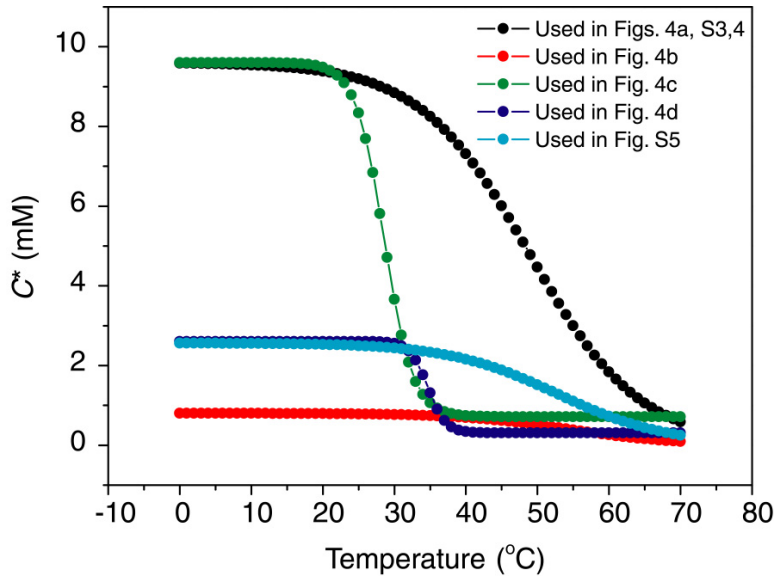

Supplementary Figure S13. C^* used in the simulations of Γ-T profiles. Inset describes that each C^* curve is used in which one of the simulated Γ-T profiles. Note that the large discrepancy of these C^* curves only arise from a small change of ρ_0 via equation (3) in the main paper and the analysis shown in Fig. S12 and equations (S13)–(S15).

S8.2 Determination of C_{max} as a function of temperature during Γ-T profiling

Let us go back to the Γ-T profiling procedure shown in Fig. S1. Assume $C_i(t) = C_{o,i}$ before the DNA channels are opened in the ith measurement cycle of Γ-T profiles, where i is a positive integer. The temperature change during the measurement will release thionine into ADNC and result in the change of $C_i(t)$ by a functional form $C_i(t) = C_{m,i}(1 - \exp(-t/\tau)) + C_{o,i}$. So the expected maximum value of $C_i(t)$ in such a measurement is $C_{max,i} = C_{m,i} + C_{o,i}$, which is used to be compared with C^* to judge whether the $C(t)$ is able to open the DNA channels in such a measurement. Figure S14 (red circles) shows the C_m as a function of temperature that is used in the simulation of Γ-T profiles. However, when the DNA channels are opened in the thionine pumping, the release C_m of thionine from PDC should be enhanced because the loss of thionine from ADNC can change the reaction equilibrium of PDC-thionine complex decomposition to promote the decomposition, as shown by the black circles of Fig. S14. Note that C_m corresponding to the case of opened DNA channels should not be used to judge whether the $C(t)$ is able to open the DNA channels in such a measurement, because if the DNA channels are not opened the C_m cannot reach that high values.

The data shown in Fig. S14 are calculated from the Γ-T profile of the open-state ADNC (shown in black circle in Fig. 1d of the main paper), by the method as described as follows. Consider the equilibrium constant K_i of the chemical reaction, PDC-thionine $\rightleftharpoons$ PDC + thionine, at temperature $T = i\Delta T$ during the ith measurement cycle of a Γ-T profile, where i is a non-negative

© 2007 Nature Publishing Group

integer, i = 0, 1, 2, …, 10. In the case of open-state ADNC, $K_i = (\sigma - \sigma_i)\,\sigma_{TH,i}/\sigma_i$, where σ is the area density of PDC monolayer, σ_i is the area density of thionine-bound PDC among the PDC monolayer, $\sigma_{TH,i}$ is the area density of free thionine near the PDC monolayer. In the case of closed-state ADNC, $K_i = (\sigma - \sigma'_i)\sigma'_{TH,i}/\sigma'_i$, where σ'_i is the area density of thionine-bound PDC among the PDC monolayer, $\sigma'_{c,i}$ $\sigma'_{TH,i}$ is the area density of free thionine near the PDC monolayer. Thus we have a series of equations

$$(\sigma - \sigma_i)\,\sigma_{TH,i}/\sigma_i = (\sigma - \sigma'_i)\,\sigma'_{TH,i}/\sigma'_i\,, \qquad \text{(S16)}$$

where the data of the left term are well obtained from the Γ-T profile of the open-state ADNC. And $\sigma'_{TH,i}$ in the right term can be solved by the recursion relations

$$\sigma'_{i+1} - \sigma'_i = \sigma'_{TH,i+1} - \sigma'_{TH,i}, \qquad \text{(S17)}$$

whereas σ'_0 and $\sigma'_{TH,0}$ are readily known from experimental data. Note that $\sigma'_{i+1} - \sigma'_i = C_{m,i+1}\Delta h = C_m((i+1)\Delta T)$, where Δh is the small height of space near PDC monolayer where free thionine inside the ADNC can readily participate into the surface-based chemical reaction. Equation (S16) can also be used to determine the C_m corresponding to opened DNA channels, only modifying equation (S17) as $\sigma'_{i+1} - \sigma'_i = \sigma'_{TH,i+1} - \sigma'_{TH,i} + h(C_{o,i+1} - C_{c,i+1})$. We emphasize that only one set of the C_m function, as shown in Fig. S14, is used in all the Γ-T simulation of Fig. 4 in the main paper and Figs. S3–S5.

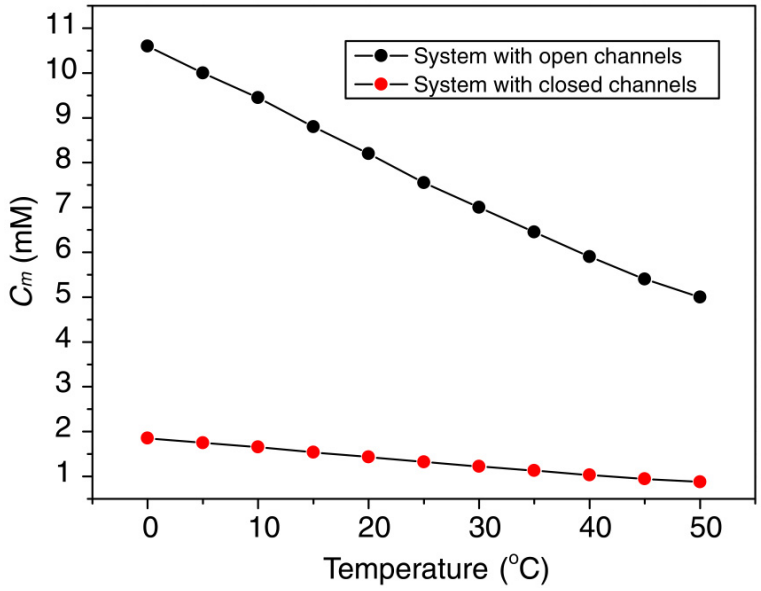

Supplementary Figure S14. C_m used in all the simulations of Γ-T profiles. C_m is the maximum concentration of thionine released from PDC monolayer at a temperature during the Γ-T profiling. When the DNA channels are all closed, the release of thionine from PDC monolayer should be quite small. The result of this case is shown as red circles. On the contrary, when the DNA channels are opened in the thionine pumping, the release of thionine from PDC should be enhanced because the loss of thionine from ADNC can change the reaction equilibrium of PDC-thionine complex decomposition to promote the decomposition, as shown by the black circles. The two curves roughly give high and low limits of the C_m in a practical case. The data are calculated from the Γ-T profile of the open state of the system based on equations (S16) and (S17).

S8.3 Simulation algorithm of Γ-T profile

© 2007 Nature Publishing Group

Actually, Figure S1 clearly shows the main scheme of the simulation algorithm of Γ-T profile. A detail is readily presented as following:

Step 1: Set the initial quantity of thionine confined inside ADNC at T_c, as well as initiate all other fixed parameters (Table 1 in the main paper), including C^* and C_m;

Step 2: The temperature is increased by a small step ΔT = 5 ˚C, and $C(t)$ is elevated accordingly by C_m;

Step 3: Judge whether DNA channels can be opened by the elevated $C(t)$, via the criterion described in the main text, that is, the DNA channels can be opened only if $C_{max} > C^*$;

Step 4: If the DNA channels are opened, then calculate the complete flux-coupled trajectories of DNA channels by the numerical method described in Note S6. The calculated $h(C_o - C_c)$ is then subtracted from the Γ value.

Step 5: Go to Step 2.

Note S9. Modulation of Γ-T profiles in simulations and experiments

Our modeling suggests that the overall behavior of Γ-T profiles is intimately dependent of the threshold C^* and the initial quantity of thionine stored in PDC monolayer, as demonstrated in Figs. 1d, 4 of the main paper and Figs. S3–S5. The former can be modulated by switching temperature T_c and thionine concentration in incubation solution during thionine storing procedure. The later can be modulated by ionic strength, hybridization efficiency, and buffer composition. Although our experiments only involve part of the modulating parameters, all possible types of Γ-T profiles predicted by the model are observed in experiments, suggesting that the gating behaviors may be modulated simply by tuning the aforementioned parameters after the nanosystem is self-assembled well. While we have described the fundamental mechanism that gives rise to polymorphism of Γ-T profiles shown in both the main paper and this supplementary document, it will be helpful to give a descriptive detail about how to achieve experimentally the polymorphism of the Γ-T profiles shown:

- **Figure 4a, S3, S4**: a high dsDNA density of about 10.0×10^{12} molecules·cm^{-2}, and a high ionic strength in Tris buffer solution (100 mM NaCl, 1 mM $MgCl_2$).
- **Figure 4b**: a relatively low dsDNA density of about 6.5×10^{12} molecules·cm^{-2} and a high ionic strength in Tris buffer solution (100 mM NaCl, 1 mM $MgCl_2$).
- **Figure 4c**: a high dsDNA density of about 10.0×10^{12} molecules·cm^{-2} and a low ionic strength in Tris buffer solution (100 mM NaCl).
- **Figure 4d**: a relatively low dsDNA density of about 8.0×10^{12} molecules·cm^{-2} and a low ionic strength in Tris buffer solution (100 mM NaCl).
- **Figure S5**: a relatively low dsDNA density of about 7.5×10^{12} molecules·cm^{-2} and a high ionic strength in Tris buffer solution (100 mM NaCl, 1 mM $MgCl_2$).

Note that the dsDNA density termed as above refers to the local dsDNA density in a micrometer-square area, not an average over a macroscopic area. The dsDNA density is equal to the density of closed DNA channels in equilibrium among the dsDNA membrane. The method to determine the density is described in detail elsewhere[14,15]. The affection of ionic strength on the melting point and stability of dsDNA is also widely discussed in literature[30–33].

In addition, we emphasize that all experiments shown in Figs. 1d, 4a, S3, S4 are based on the same samples and experimental configuration with only changing T_c, and all corresponding simulations in Figs. 4a, S3, S4 are based on the same parameter set with only changing T_c. The

© 2007 Nature Publishing Group

strict consistency may guarantee the availability of the comparisons between the simulations and experiments. Besides the high consistency among these data, the other simulations shown in Figs. 4b-d, S5 are obtained by only varying C^* as shown in Fig. S13, which further confirms that our modeling may really capture the inherent properties of DNA channels.

© 2007 **Nature Publishing Group**

Supplementary Discussion

Minimizing the perturbation of measurements on the system behavior. The electrochemical measurements would inevitably interact with the nanosystems. This is also the major origin of the data noise and errors. For example, it is known that cyclic voltammetry (CV) would deactivate the electroactivity of thionine molecule temporarily. To minimize the measurement perturbation to our system, we employed a few strategies. First, each measurement is performed after the thionine transport events and the system reached equilibration well, in which external measurement have much less effect on both dsDNA layer and thionine inside the DNA nanocompartment, according to both our previous studies and other related literature[15-17,20,34,35]. Second, the voltage scanning range of CV is kept in a range of –0.4 ~ 0 V, which is proved not to affect the conformation of dsDNA layer[16]. Third, each measurement is performed rather quickly by manual operation with intervals minimized as possible. Fourth, after each measurement the device is immediately returned to the operation buffer to recover both the equilibrium of system and thionine's electroactivity.

Experimental limitation. Our model not only explains quantitatively the experimental observations, also predicts the detailed dynamics of single DNA channels and the corresponding excited transport flux. However, our current experimental techniques do now allow the simultaneous examination of the dynamics of single-channel and the transport flux across it. It is expected that the technical difficulty remains in future investigations.

Mathematical aspect of our theoretical modeling. One of the purposes of this work is to intimately couple single-channel gating dynamics with single-file transport dynamics, in other words, how the single-channel dynamics is affect by the non-equilibrium transport dynamics of particles through the channel. Our basic idea on this problem is to establish the connection between the two dynamics, which mathematically can solve the coupled behaviors by enabling joint consideration of both the dynamics. As the analysis described in the main paper, the dynamics of single DNA channel is dominated by the applied external force $F(t)$ (according to equation (1) in the main paper). Meanwhile, the steady sate of single-file transport flux is dominated by $C(t)$ (according to equation (5) in the main paper). Therefore, to connect the two dynamics is to establish: (*1*) the relationship between the gating of single channel and $F(t)$, (*2*) the quantitative relationship between $F(t)$ and $C(t)$. The first relationship determine in what state of single-channel the transport flux through the channel can be established, assuming that the channel's gating depends on the mechanical force that it received. This relationship is established by the proposed dual criticality picture, in which the permeability of single-channel defined by a critical radius of the channel, R^*, can lead to two critical forces (F_o, F_c) describing the opening and closing criticalities of the channels, via the hysteretic trajectories. The second relationship actually extends the first relationship from microscopic scale to macroscopic quantity, which can be used to predict experimentally testable values. Mathematically, the quantitative relationship between $F(t)$ and $C(t)$ let us to be able to jointly consider the equations (1), (2), (5) in the main paper, and simplify the three equations into one; in other words, if one know $C(t)$ or $j(t)$, one then can solve the trajectory of $\langle x(t) \rangle$. Thus, the unknown variables are simplified to find the solution of $C(t)$ or $j(t)$. This is then done in equation (6) in the main paper, and the subsequent equation (7) gives the analytic solution.

© 2007 Nature Publishing Group

Difference of physical meanings between gating threshold and trajectory-dependent dual criticality. Both the critical concentrations C_o, C_c, and the gating threshold concentration C^* are the physical consequence of R^*. However, they have remarkable different physical meanings. The critical concentrations C_o, C_c, cannot be used to judge which kind of $C(t)$ can open the channel, because C_o, C_c are trajectory dependent, whereas the trajectory is dependent of the initial condition which is always changed in each measurement step of the Γ-T profiles, as shown in the insets of Fig. 4 of the main paper. However, C^* is defined as $\partial\langle x(t)\rangle/\partial t = 0$, which corresponds to the final state ($t \to \infty$) of $C(t)$ increase by $C(t) = C_m(1 - \exp(-t/\tau)) + C_1$. C^* physically corresponds to the minimum force F^* whose work can dilate the channel to R^*. Therefore, C^* and F^* reflect the inherent properties of the channel gating, independent of the trajectory of channel's motion, and are not directly measurable in the Γ-T profiles, whereas C_o, C_c are transient and not inherent, but can be observed by their difference form of $C_o - C_c$ in the Γ-T profiles. More intuitively speaking, C^* gives rise to the diverse overall behavior (modulability, polymorphism) of the Γ-T profiles, whereas C_o, C_c give rise to the quantitative details of each data point in a Γ-T profile.

Limitation of theoretical modeling. While the theoretical modeling includes a few coarse-graining treatments, we have established a minimal model to unify the channel gating and single-file flux pumping into one picture. While being put into simplicity, the physical picture can be improved in several ways. For example, we can further ask whether the asymmetry of DNA channel during its gating could contribute nontrivial effect on the single-file transport, whether the critical radius shifts according to the concentration gradients or other physical perturbation, how important the noise can play a role in the non-equilibrium channel gating, and so on. One would notice that these questions raise nontrivial tasks to find appropriate answers which are substantially beyond one paper. Thus, they remain for future studies.

Ratchet-like mechanism. Based on our modeling, we identify both channel's gating and solute permeation as a ratchet-like mechanism. For the channel's gating, the symmetry breaks for both closed state and opened state. At the closed state, the channels with ground energy are faced with asymmetric steric constraints (as shown in Fig. 2a of the main paper) in both directions, where $R(t)$ is more easier to increase than to decrease. Also, the symmetry breaking between channel's dilation (increase of $R(t)$) and shrinkage (decrease of $R(t)$) occurs when the channel is opened with thionine flux established. This lack of symmetry reflects the intuitive picture that opened channels move more easily along the direction of $R(t)$ decrease than the direction of $R(t)$ increase. This spatial breaking symmetry of channel's motion then leads to breaking of time-reversal symmetry of transport flux via spontaneous changes of channel-particle interaction. Intuitively speaking, the solute flux tend to decrease in most time during the channel's opening due to that the solute permeation is against the higher deformation potential of DNA channels. Our computations shown in Fig. 2 and Fig. 4 of the main paper clearly show this time-reversal symmetry breaking, resulting in ratchet-like oscillations of $j(t)$, $R(t)$, and $F(t)$. Thus, the typical entire potential profile of a thionine molecule moving along a single DNA channel depicted in Fig. S8 (lower panel) is a function of time during the channel's gating, with the same periodic changes as $j(t)$ and $F(t)$.

What properties are important for solute molecules that can transport DNA channels as a mechanism described in this study? Previous works have shown that the molecular encaging effect of ADNCs (that is, small molecules of suitable sizes can be encaged inside ADNC) is a generic property of ADNC, and is nonspecific to certain species[15,20]. Although this study only used

© 2007 Nature Publishing Group

thionine, it is possible that other small molecules can also be used as transporter solute once if the way to regulate their concentration inside ADNC is found. According to our model, the size is the major consideration of solutes that could be transported cross the channels. We believe those minor properties like charge or hydrophobicity (or hydrophilicity) should have detailed effects on the transport behavior. However, our modeling shows that those minor properties have much less effect on the major character of transport-flux-coupled gating of the channel which is described in the main text. This is because the properties like charge or hydrophobicity are mainly reflected in the parameters (p and n_m) in equation (2) and the parameters (A_1 and A_2) in equation (5) of the main text. But our major calculation results shown in Fig. 2 and Fig. 4 of the main paper are much less sensitive to these parameters around the value shown in Table 1.

Implication of the modeling on the design of DNA channels system. The theoretical modeling also provides a general framework for the *in silico* rational design of DNA channels system. The equation (1) in the main text means that two physical properties of the DNA channels are crucial for their gating dynamics and may be designed by DNA sequences and nanostructures: the conformational diffusion coefficient (D), and the area tension (α) on the circumference of the channels. D usually decreases with increasing the weight of single DNA motif that forms the DNA channels[36], as well as is related to the geometrical shape of DNA motifs and the connection fashion between the DNA motifs. α is determined by the interaction between the DNA motifs. Both of the properties are designable by the structure of DNA motifs, which is programmable from DNA sequences. For example, the structure of DNA motifs could be four-stranded i-motif structure[20], G-quadruplex DNA[37], and four-stranded paranemic crossover DNA[38], etc. The different structures give rise to distinct flexibility and stiffness of DNA motifs and distinct interaction energy between the DNA motifs, thus leading to distinct D and α. This may provide us a versatile means to program the physical properties of DNA channels, as well as their inherent gating dynamics.

© 2007 Nature Publishing Group

References

1. Gillespie, P. G. & Walker, R. G. Molecular basis of mechanosensory transduction. *Nature* **413**, 194–202 (2001).
2. Yellen, G. The voltage-gated potassium channels and their relatives. *Nature* **419**, 35–42 (2002).
3. MacKinnon, R. Potassium channels and the atomic basis of selective ion conduction (nobel lecture). *Angew. Chem. Int. Ed.* **43**, 4265–4277 (2004).
4. Perozo, E., Cortes, D. M., Sompornpisut, P., Kloda, A. & Martinac, B. Open channel structure of MscL and the gating mechanism of mechanosensitive channels. *Nature* **418**, 942–948 (2002).
5. Yang, H. *et al*. Protein conformational dynamics probed by single-molecule electron transfer. *Science* **302**, 262-266 (2003).
6. Cherstvy, A. G. & Winkler, R. G. Complexation of semiflexible chains with oppositely charged cylinder. *J. Chem. Phys.* **120**, 9394–9400 (2004).
7. Cherstvy, A. G., Kornyshev, A. A. & Leikin, S. Torsional deformation of double helix in interaction and aggregation of DNA. *J. Phys. Chem. B* **108**, 6508–6518 (2004).
8. Kornyshev, A. A. & Leikin, S. Sequence recognition in the paring of DNA duplexes. *Phys. Rev. Lett.* **86**, 3666–3669 (2001).
9. Wiggins, P. A. *et al*. High flexibility of DNA on short length scales probed by atomic force microscopy. *Nature Nanotechnology* **1**, 137–141 (2006).
10. Wiggins, P. & Phillips, R. Analytic models for mechanotransduction: Gating a mechanosensitive channel *Proc. Natl. Acad. Sci. USA* **101**, 4071–4076 (2004).
11. Markin, S. & Sachs, F. Thermodynamics of mechanosensitivity. *Phys. Biol.* **1**, 110–124 (2004).
12. Goychuk, I. & Hänggi, P. Ion channel gating: a first-passage time analysis of the Kramers type. *Proc. Natl. Acad. Sci. USA* **99**, 3552–3556 (2002).
13. Risken, H. *The Fokker-Planck equation* (2nd ed. Springer, New York, 1989).
14. Peterson, A. W., Heaton, R. J. & Georgiadis, R. M. The effect of surface probe density on DNA hybridization. *Nucleic Acids Res.* **24**, 5163-5168 (2001).
15. Mao, Y. *et al*. Reversibly switchable DNA nanocompartment on surfaces. *Nucleic Acids Res.* **32**, e144 (2004).
16. Kelley, S. O. *et al*. Orienting DNA helices on gold using applied electric fields. *Langmuir* **14**, 6781–6784 (1998).
17. Boon, E. M., Ceres, D. M., Drummond, T. G., Hill, M. G. and Barton, J. K. Mutation detection by electrocatalysis at DNA-modified electrodes. *Nature Biotechnol.* **18**, 1096-1100 (2000).
18. Strey, H. H. *et al*. Refusing to twist: demonstration of a line hexatic phase in DNA liquid crystals. *Phys. Rev. Lett.* **84**, 3105–3108 (2000).
19. Chou, T. How fast do fluids squeeze through microscopic single-file pores? *Phys. Rev. Lett.* **80**, 85–88 (1998).
20. Mao, Y. *et al*. Alternating-electric-field-enhanced reversible switching of DNA nanocontainers with pH. *Nucleic Acids Res.* doi: 10.1093/nar/gkl1161 (2007).
21. Kollmann, M. Single-file diffusion of atomic and colloidal systems: asymptotic laws. *Phys. Rev. Lett.* **90**, 180602 (2003).
22. Levitt, D. G. Dynamics of a single-file pore: non-Fickian behavior. *Phys. Rev. A* **8**, 3050-3054

© 2007 **Nature Publishing Group**

(1973).

23. Lutz, G., Kollmann, M. & Bechinger, C. Single-file diffusion of colloids in one-dimensional channels. *Phys. Rev. Lett.* **93**, 026001 (2004).
24. Hahn, K., Kärger, J. & Kukla, V. Single-file diffusion observation. *Phys. Rev. Lett.* **76**, 2762-2765 (1996).
25. Lin, B., Meron, M., Cui, B. & Rice, S. A. From random walk to single-file diffusion. *Phys. Rev. Lett.* **94**, 216001 (2005).
26. Eisenberg, R. S., Klosek, M. M. & Schuss, Z. Diffusion as a chemical reaction: stochastic trajectories between fixed concentrations. *J. Chem. Phys.* **102**, 1767–1780 (1995).
27. Nadler, B., Schuss, Z. & Singer, A. Langevin trajectories between fixed concentrations. *Phys. Rev. Lett.* **94**, 218101 (2005).
28. Kosztin, I. & Schulten, K. Fluctuation-driven molecular transport through an asymmetric membrane channel. *Phys. Rev. Lett.* **93**, 238102 (2004).
29. Chou, T. & Lohse, D. Entropy-driven pumping in zeolites and biological channels. *Phys. Rev. Lett.* 82, 3552–3555 (1999).
30. Várnai, P. & Zakrzewska, K. DNA and its counterions: a molecular dynamics study. *Nucleic Acids Res.* **32**, 4269-4280 (2004).
31. Denisov, V. P. & Halle, B. Sequence-specific binding of counterions to B-DNA. *Proc. Natl. Acad. Sci. USA* **97**, 629-633 (2000).
32. Korolev, N., Lyubartsev, A. P. & Nordenskiöld, L. Application of polyelectrolyte theories for analysis of DNA melting in the presence of Na^+ and Mg^{2+} ions. *Biophys. J.* **75**, 3041-3056 (1998).
33. Owczarzy, R., Dunietz, I., Behlke, M. A., Klotz, I. M. & Walder, J. A. Thermodynamic treatment of oligonucleotide duplex-simplex equilibria. *Proc. Natl. Acad. Sci. USA* **100**, 14840-14845 (2000).
34. Kelley, S. O., Barton, J. K., Jackson, N. M. & Hill, M. G. Electrochemistry of methylene blue bound to a DNA-modified electrode. *Bioconjugate Chem.* **8**, 31-37 (1997).
35. Mao, Y., Luo, C. & Ouyang, Q. Studies of temperature-dependent electronic transduction on DNA hairpin loop sensor. *Nucleic Acids Res.* **31**, e108 (2003).
36. Smith, D. E., Perkins, T. T. & Chu, S. Self-diffusion of an entangled DNA molecule by reptation. *Phys. Rev. Lett.* **22**, 4146-4149 (1995).
37. Alberti, P. & Mergny, J.-L. DNA duplex-quadruplex exchange as the basis for a nanomolecular machine. *Proc. Natl. Acad. Sci. USA* **100**, 1569-1573 (2003).
38. Yan, H., Zhang, X., Shen, Z. & Seeman, N. C. A robust DNA mechanical device controlled by hybridization topology. *Nature* **415**, 62-65 (2002).

© 2007 **Nature Publishing Group**